A PROJECT REPORT ON

Analysis to find best DC-DC converter for an electric vehicle

Submitted in partial fulfillment for the requirement of the award of

PROJECT BASED SUMMER INTERNSHIP PROGRAM 2024 **IN** ***HYBRID ELECTRIC VEHICLES***

HOSTED BY

TIH IIT ROORKEE (SUPPORTED BY DST Govt. of India)

SUBMITTED BY

SHASHANK CHANDRAVANSHI

(DEPARTMENT OF ELECTRICAL ENGINEERING MADHAV INSTITUTE OF TECHNOLOGY & SCIENCE, GWALIOR (M.P.) – 474005)

UNDER THE GUIDANCE OF

MR. ASHISH JHA

17 JUNE 2024 – 01 AUGUST 2024

ACKNOWLEDGEMENT

First of all, I thank the supreme power God Almighty for his blessings.

With utmost sincerity, I articulate my profound gratitude sincere thanks to **MR. ASHISH JHA**, *for his adroit guidance, inexplicable assistance and unrelaxed support help to carry out this project successfully.*

My heartful thanks and gratitude to family members and friends for their affectionate blessings and inexplicable enthusiasm to finish this project successfully.

SHASHANK CHANDRAVANSHI

CONTENTS

Abstract

A DC-DC converter for an electric car is designed in this work. The DC-DC converter has an adjustable output of 12–15 V and an input range of 200–400 V, which together yield 500W. Sales of electric vehicles are starting to gather up steam, and there's still a need—particularly for single-seater class vehicles—for DC-DC converters to extract power from the tractive system. Furthermore, future DC-DC converter designs can benefit from increased efficiency without compromising a large input voltage range. Finally, the design and testing of a forward active clamp DC-DC converter has been completed. Matlab scripts, LTSpice simulations, and spreadsheet calculators were also developed to help with DC-DC work.

1. Introduction

There are currently major issues with the environment and human life as a result of the vast number of automobiles in use globally. These days, there are three major issues: air pollution, warming of the planet, and the rapid depletion of petroleum reserves. It has frequently been predicted that electric vehicles (EVs), hybrid electric vehicles (HEVs), and fuel cell electric vehicles (FCEVs) will soon replace conventional cars. Most electric and hybrid electric designs use one of two energy storage systems: the "rechargeable energy storage system" (RESS), which has a high power capability and reversibility, or the "main energy system" (MES), which has a high energy storage capacity. While MES offers a greater driving range, RESS provides powerful acceleration and regenerative braking. The high voltage of the DC-link presents considerable hurdles for vehicle designers when connecting energy storage and supply devices with traction systems. Energy storage and supply devices fluctuate in output voltage depending on the load or state of charge. DC-DC converters can be used to link the parts of the electric power train by raising or lowering the voltage levels. The vehicle industry's constraints dictate that power converter construction must be dependable, lightweight, compact, highly efficient, and free of electromagnetic interference and current and voltage ripple.

Thus, a comparative analysis of 3-DC/DC converter topologies—the conventional step-up dc-dc converter, the Full-Bridge step-up dc-dc converter, and the interleaved 4-channel step-up dc-dc converter with independent inductors—is done in this chapter. Each topology's modeling and control are demonstrated. For every layout, 30KW DC/DC converter simulations are performed. This analysis considers each converter topology's weight, volume, waves in current and voltage, electromagnetic interference (EMI), and efficiency. When a car runs on electricity, it's considered electric using a mix of energy sources, including batteries, supercapacitors, and fuel cells (FCs). An electric vehicle's primary energy source is supported by one or more energy storage units. By doing this, the system's cost, mass, and volume can be decreased while maintaining a notably greater level of performance. Batteries and SCS are the two most widely used energy storage systems. The fuel cell stack can be connected to them in a variety of ways. It's simple to connect two devices directly in parallel (FC/battery, FC/SC, or battery/SC).

The impedance of the devices, however, passively determines the amount of power that is drawn from each one and cannot be changed in this way. Many factors affect the impedance, including temperature, charge level, condition, and operating point. Due to this, each gadget may be used in an inappropriate manner, for example, in terms of efficiency or health. Just a tiny portion of the two devices' operational range might be utilized since the two devices' voltage characteristics need to match exactly. For instance, in a battery/supercapacitor combination, the fuel cell's set voltage means that it must always supply almost the same amount of power, and only a small percentage of the supercapacitor's energy exchange capacity can be utilized. Again, this is due to the nearly constant voltage of the battery. By using DC/DC converters, one may control each device's power and select how much each device's voltage varies (Schaltz & Rasmussen, 2008).

2. Design Requirements

The project's technical design requirements are explained in this chapter. It includes standards for both physical dimensions and electrical performance.

Technical Requirements

- **Input Voltage Range**

An input voltage range of 200–400 VDC is required for the design. Under typical operating conditions, the tractive system voltage will fluctuate between 220V and 369V due to the 88s8p Li-Ion battery setup. By increasing the range to 200–400V and adding a 20–V safety buffer is possible.

- **Adjustable Output Voltage**

In order to work with the low voltage battery, an adjustable output voltage of 12–15V is required. The nominal voltage of the low voltage battery used ranges from 11.2 to 14.4V. A minimum operating voltage of 12V is acceptable since Cal Poly Racing is not expecting the LV battery dropping to the required 11.2V level of charge.

- **Control and Sense Ports**

To ensure safe operation, DC-DC converter voltage and current data must be able to be continuously monitored. Cal Poly Racing additionally anticipated an externally controlled variable output voltage.

- **Continuous Output Power Rating**

In an endurance race, Cal Poly Racing plans to use up to 400W of 12V power. Although the power consumption varies during the race, the high power "bursts" might last for many minutes, necessitating a 500W continuous power rating.

- **Input/Output Overcurrent Protection**

There is an ongoing flow of new members at Cal Poly Racing. Because of this, mistakes happen during assembly and operation that project managers have no way to entirely prevent. This makes output short circuits a potential occurrence. Overcurrent protection needs to be included in the design in order to safeguard both the DC-DC and the linked harness.

- **Input/Output Overvoltage Protection**

Regenerative braking or a linked voltage source with an improper setting could result in an overvoltage problem. To avoid having to buy a replacement DC-DC, the DC-DC must safeguard itself.

- **Input/Output Reverse Voltage Protection**

As previously stated, errors in assembly and operation may occur during the DC-DC's lifetime. Reverse voltage errors are another frequent mistake that happens. Due to the device's dual-sided battery-powered energy sources, these occurrences may happen at both the input and output. To ensure dependable operation, the device must be able to tolerate input and output reverse voltage during a failure without suffering permanent harm.

- **Rated for Automotive Conditions**

When the device is used in a moving car, it experiences strong vibrations. Thus, AEC-Q100 rated or higher should be applied to most, if not all, of the components.

- **Isolated Design**

LV and HV are on separate, clearly defined PCB parts, per EV.6.1.7, the 2019 Formula SAE Electric rules. Under conformal coating, there is a space between traces that is larger than 4 mm. UL-certified, moisture-resistant insulating materials rated for 150 degrees Celsius or more are used to separate HV and LV inside an enclosure, and EV.6.1.5 specifies that the air space be greater than 30 mm. Furthermore, the design is isolated at this power level to guard against low voltage component damage in the event of a breakdown.

- **IP31 Rated**

The device satisfies EV.6.5.3 of the 2019 Formula SAE Electric requirements and is moisture-protected with an approximate IP31 certification. This indicates that the device is resistant to dripping water and larger than 2.5mm probes. During the rain test, the car will be splashed with water directly; however, the DC-DC converter's battery box shell will shield it from the spray.

- **Small Volume**

Because Cal Poly Racing needs fewer components to maximize vehicle packaging, the DC-DC converter must be around half the size of the Meanwell RSP-500-15 DC-DC converter, which means physical size smaller than 115mm x 127mm x 40.5mm.

- **Lightweight**

The DC-DC module must weigh a lot less than the RSP-500-12's 2.866 lbs in order to serve as a useful substitute for the current module. It is suitable to aim for a total weight of less than 2 pounds.

- **Efficiency**

Because of the above specifications, the converter must have an overall efficiency of at least 90%. In relation to the overall power usage, the losses by the LV system are minimal.

- **Line and Load regulations**

Because the DC-DC converter must function in a wide voltage and load range, strict line and load regulation is required to keep the voltage from deviating too much from the nominal value. The line and load regulations were both set at a maximum of 5%.

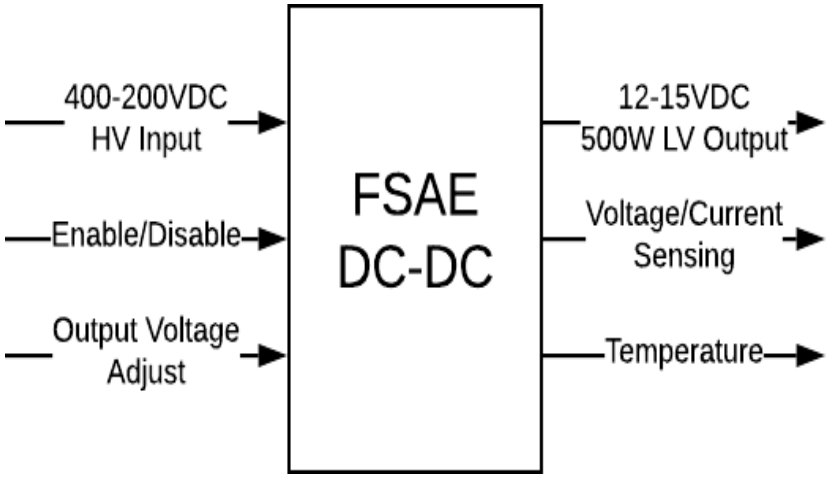

Figure 1: Level-0 Block Diagram

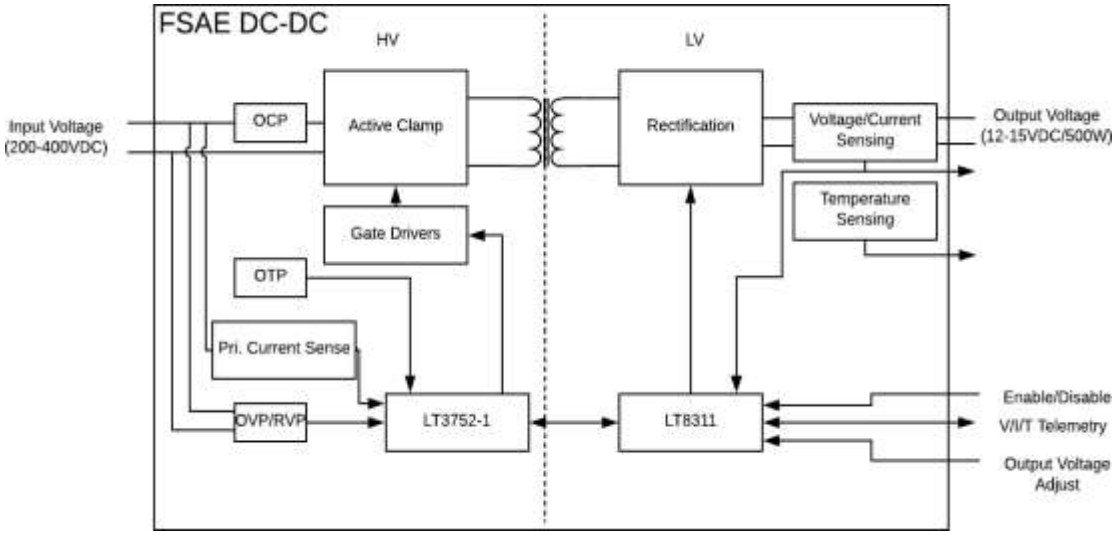

Figure 2: Level-1 Block Diagram

Three inputs and three outputs make up the suggested system, as shown by the project's Level 0 block diagram. The three inputs are the "high voltage" input, the DC-DC converter enable control, and the converter output voltage adjustment. The voltage/current sensing signals, different temperature indications, and the "low voltage" output are all contained in the three outputs.

The principal building blocks on both sides of the division make up the project's Level 1 block diagram, which is shown in Figure 2. This comprises the two controller ICs, the active clamp circuitry, different operational protections, and different sensor blocks.

Table 1: Enumerates the project's design needs.

Table 1: Requirements List

Requirements	Value
Input voltage range	200 to 400V
Output Voltage Range	12 to 15V
Efficiency	> 90%
Additional Features	Control, Sense Ports
Power Rating	Continuous 500W
Input/Output Protection	Overvoltage, Overcurrent and Reverse Voltage Protection
Ratings	IP31, Vibration Resistant, Isolated
Size	< 115mm x 127mm x 40.5mm
Weight	2-lbs.

- **Electric vehicles powertrain**

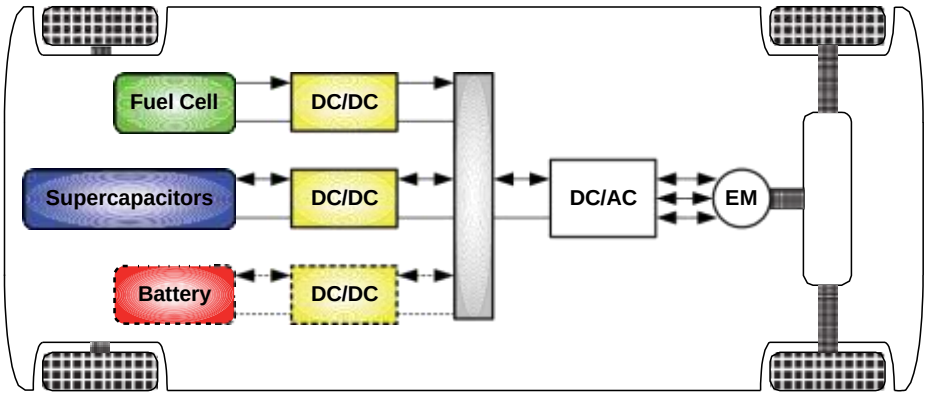

Figure 4: Electric vehicle drive system

3. DC/DC converters for electric vehicles

The many designs of EV power supplies show that at least one DC/DC converter is needed to interface the FC, battery, or supercapacitors module to the DC-link. In the field of electric engineering, a DC to DC converter—also referred to as a power converter—is a kind of electric circuit that modifies the voltage level of a direct current (DC) source by holding onto input energy for a brief period of time before releasing it to the output at a different voltage. The storage may be included in either electric field storage (capacitors) or magnetic field storage (inductors, transformers) components. Power can only be transferred from the input to the output by DC/DC converters in a single direction. However, bi-directional DC/DC converter topologies are possible for nearly all of them. In situations where regenerative braking is necessary, a bi-directional converter's The capacity to distribute power both ways is advantageous.

The duty cycle, which is the ratio of the on/off timings of the switch, can be adjusted to control the amount of power that flows from the input to the output. Usually, this is done to modify the output voltage, input current, and output current or to keep the power constant. Isolation between the input and the output may be provided by converters that use transformers as their foundation. Electronic noise, complexity, and high cost for certain topologies are the main drawbacks of switching converters. Numerous types of DC/DC power converters have been discussed in the literature (Chiu & Lin, 2006; Fengyan et al., 2006).

3.1 Electric vehicle converters requirements

The DC/DC converter is used to manage the DC-link voltage and boost the fuel cell's voltage when it is connected. However, a reversible DC/DC converter is needed in order to interface the SCs module. DC-DC converter topologies have been proposed in a number of various ways (Lachichi & Schofield, 2006; Yu & Lai, 2008; Bouhalli et al., 2008). Direct energy conversion structures and intermediate storage component architectures (with or without transformer coupling) are examples of these topologies. However, for automotive applications, the following design factors are crucial:

- Light weight,
- High efficiency,
- Small volume,
- Low electromagnetic interference,
- Low current ripple drawn from the Fuel Cell or the battery,
- The step up function of the converter,
- Control of the DC/DC converter power flow subject to the wide voltage variation on the converter input.

4. Designing and Simulation Results

For the project, the Active Forward Clamp Controller (LT3752-1) from Linear Technology satisfies every design criteria. The IC features a housekeeping controller and can do ZVS. ZVS enhances switching efficiency, and by eliminating the requirement for an extra IC, the housekeeping controller shrinks the board's size. Furthermore, The LT8311 Opto-Coupler Driver Synchronous Rectifier Controller for Forward Converters and the LT3752 are integrated from the factory. Efficiency is increased by synchronous rectification, which is made possible by this.
Component values were calculated using Excel calculators.

The switching frequency of the LT3752 Demo Board is 100 kHz, while our DC-DC converter has a 300 kHz switching frequency, which is lower than other designs currently in use. We are able to carry 2.5 times the power while maintaining a similar size to the demo board because of this greater switching frequency.

Inductor Output:

$$L_{OUT} = \frac{V_{OUT}}{\Delta I_L \cdot f_{OSC}} \cdot \left(1 - \frac{V_{OUT}}{V_{IN}} \frac{N_p}{N_s}\right)$$

L_{OUT} = output inductance
V_{OUT} = output voltage
ΔI_L = output current ripple (peak-to-peak)
f_{OSC} = switching frequency
V_{IN} = input voltage
N_p = number of primary turns
N_s = number of secondary turns

Equation 1: Based on the Output Current Ripple, the Output Inductor Value

The output current ripple is initially intended to be 40% of IOUT(MAX), however it was increased because the available inductors in our desired size had continuous and saturation current ratings. The LT3752-1's programmable slope correction option ought to offset the higher current ripple.

4.1 Active Clamp Switch Timing

Programming delays between AOUT, the clamp MOSFET gate signal, and OUT, the primary MOSFET gate signal (tAO), as well as OUT to AOUT (tOA), are necessary for ZVS for the primary MOSFET. The clamp gate signal rising edge delay to the primary gate signal falling edge delay, or clamp MOSFET turn-off to primary MOSFET turn-on, is programmed to produce both timings using a single resistor (RTAO).

$$t_{AO(min)} = t_{AOUT(fall)} + t_{GDHL} + t_{ClpD(off)} + t_{Clp(fall)} - (t_{PriD(on)} + t_{Pri(rise)})$$

$t_{AOUT(fall)}$ = clamp gate signal fall time
t_{GDHL} = gate driver high-to-low
$t_{ClpD(off)}$ = clamp delay off time
$t_{Clp(fall)}$ = clamp fall time
$t_{PriD(on)}$ = primary delay on time
$t_{Pri(rise)}$ = primary rise time

Equation 2: Minimum Time (Clamp Off, Primary On) between AOUT and OUT

Using the chosen MOSFETs datasheet signal delay values, the shortest amount of time between the clamp gate signal and the primary gate signal is calculated. A higher tAO value enables the magnetizing current of the main transformer to lower the main MOSFET's drain voltage in the direction of VIN before turning it on.

$$R_{TAO} = \left(\frac{t_{AO} - 50ns}{3.8ns}\right) \cdot 1k\Omega$$

Equation 3: Timing Change from AOUT to OUT Resistor

The tOA value is automatically generated and validated to make sure that the clamp MOSFET does not activate until the primary and forward MOSFETs are turned off in order to prevent shoot-through.

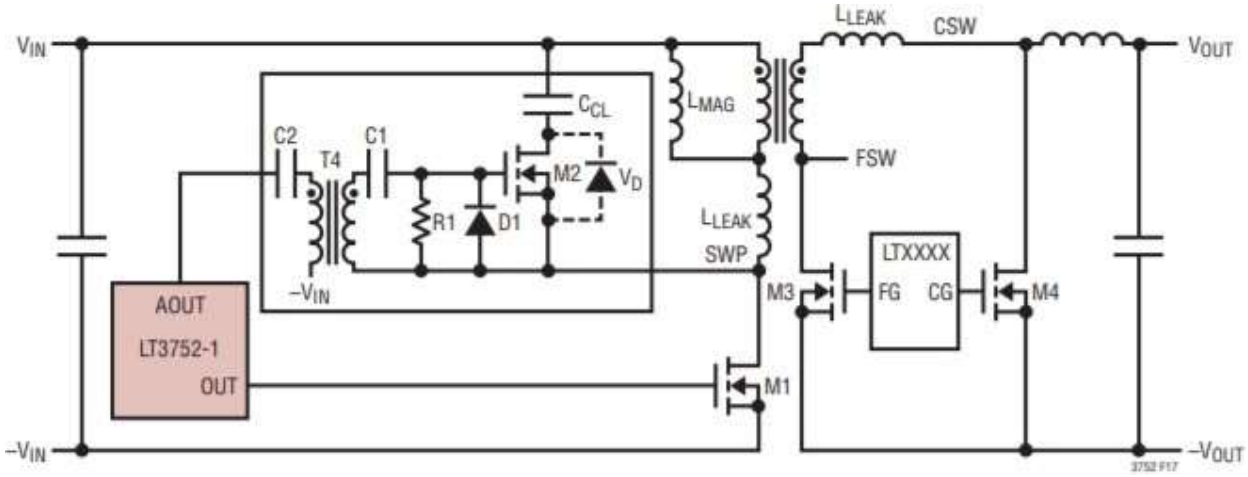

Figure 8: Switch Configuration

The primary MOSFET is denoted by M1, the clamp MOSFET by M2, the forward MOSFET by M3, and the catch MOSFET by M4.

4.2 Synchronous Rectifier Timing

To synchronize the primary switching to the secondary side synchronous rectification, SOUT, the control signal to the secondary side, to OUT (tSO), and OUT to SOUT (tOS), must be set for maximum efficiency. Two resistors produce these two timings: RTAS programs the catch gate signal falling edge to the primary gate signal rising edge delay, and RTOS programs the primary gate signal falling edge to the catch gate rising edge delay, or primary MOSFET turn-off to catch MOSFET turn-on.

$$t_{SO(min)} = t_{SOUT(fall)} + t_{SyncD} + t_{CchD(off)} + t_{Cch(fall)} - (t_{OUT(rise)} + t_{PriD(on)} + t_{Pri(rise)})$$

$t_{SOUT(fall)}$ = sync signal fall time

t_{SyncD} = synchronous transformer delay

$t_{CchD(off)}$ = catch delay off time

$t_{Cch(fall)}$ = catch fall time

$t_{OUT(rise)}$ = primary rise time

Equation 4: Minimum Time (Catch Off, Primary On) from SOUT to OUT

Using the chosen MOSFETs datasheet signal delay values, the shortest period of The calculation of the interval between the primary gate signal and the catch gate signal. For continued conduction, When the primary MOSFET is turned off, the catch MOSFET needs to be turned on at all times. As a result, the non-overlap intervals between the SOUT & OUT gate signals are incredibly brief.

$$t_{AS} = t_{AO} - t_{SO}$$

Equation 5: Minimum Time (Clamp Off, Primary On) between AOUT and OUT

After the tSO value is found, the tAS value is found to set the clamp off to primary on delay. The tSO delay is defined by the individual timings of the AOUT to OUT and AOUT to SOUT.

5. Design, modeling, control and simulation results of 3 DC/DC converters

The Simpower tools of Matlab/Simulink are used to model the examined converters, considering the losses in inductors, capacitors, and diodes in addition to IGBT and diode characteristics (actual components). As seen in Fig. 11, two control loops are used to provide precise voltage regulation. This control approach (current mode control) requires the inner loop to adjust the inductor current. The outer loop commands the required current, which controls the output voltage error. RST controllers were used for the control.

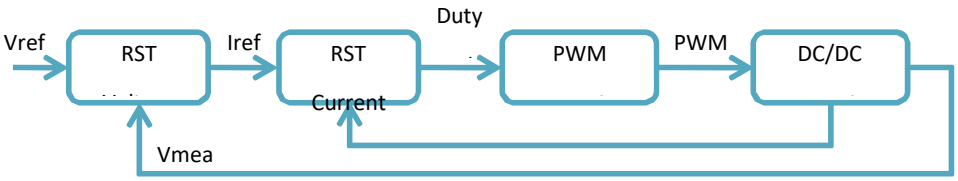

Figure 11: Control mode Block diagram

5.1 RST controller

The conventional structure of the RST controller is shown in Figure 12. This structure has two degrees of freedom: first, the design of digital filters R and S achieves the desired regulation performance, and second, the design of digital filter T achieves the desired tracking and regulation. With this system, tracking and regulating performance levels may be achieved at different levels. When a controller acts on the regulation error, it is not possible to independently specify tracking and regulation performance. This is known as T=R. Additionally, a digital PID controller may be expressed using this form, which provides options for R, S, and T (Landau, 1998).

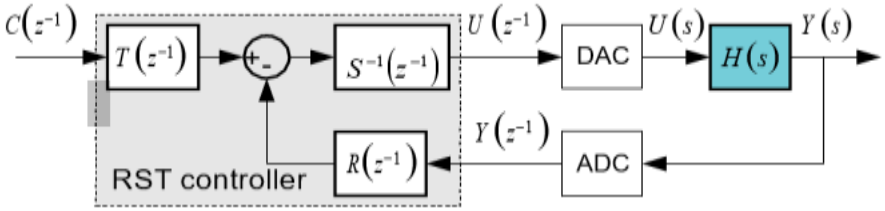

Figure 12: The digital controller's RST canonical structure

5.2 Boost DC/DC converter

A boost DC/DC converter (often called a step-up converter, as shown in Fig. 13) is a power converter that produces an output DC voltage that is greater than its input DC voltage. This kind of switching-mode power supply consists of a minimum of two semiconductor switches (a diode and a switch) and a minimum of two energy storage elements (an inductor or capacitor). In order to reduce output voltage ripple and output current ripple, the converter's output is supplemented by capacitor-based filters and an inductor connected in series with the input DC source.

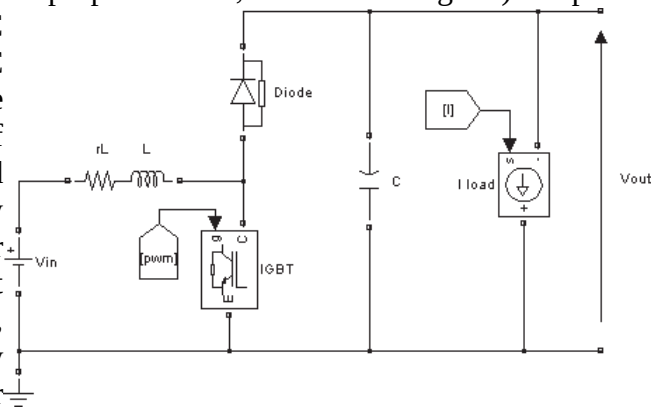

Figure 13: Standard step-up DC-DC converter.

(a). The inductor current loop is shown in Fig. 14.

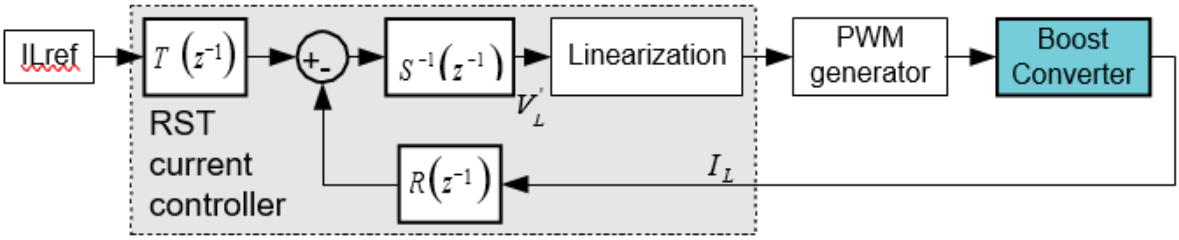

Figure 14: Boost converter inductor current loop

(b). The output voltage control loop is shown in Fig. 15.

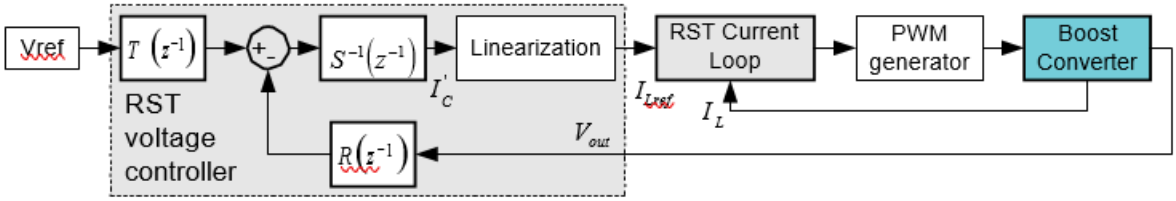

Figure 15: Boost converter output voltage control loop

Simulation results

There are ripples in the voltage and current of roughly 2 volts and 10 amps, respectively. The outcomes demonstrate that, as a result of effective regulation, the converter responds to power demands.

Fig. 16 illustrates the boost dc/dc converter's efficiency at full load, which is around 83%.

As explained in the section "Electromagnetic compatibility regulation," Fig. 17 shows the output signal spectrum of the LISN. It is evident that the converter's degree of conducted interference is above what the standards would allow. Thus, suppression of the EMI filter is necessary to meet regulatory requirements.

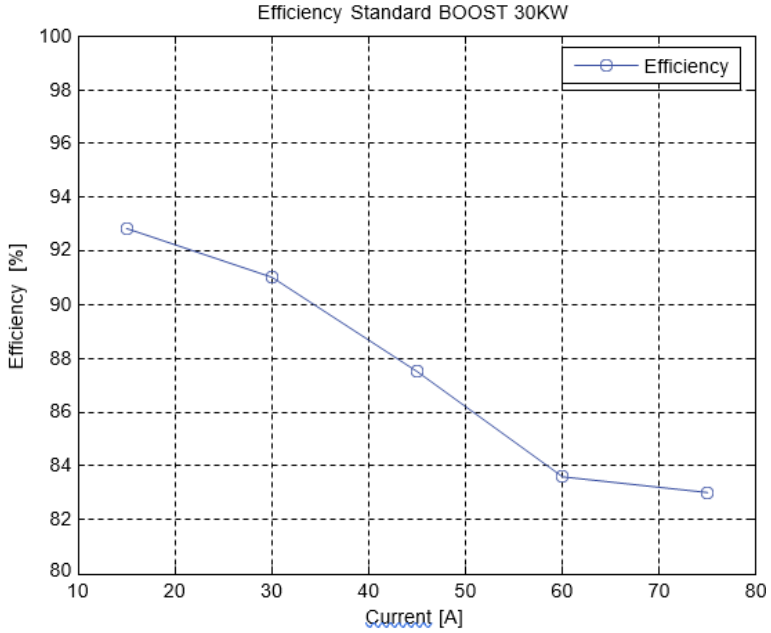

Figure 16: Improve converter performance in relation to current load

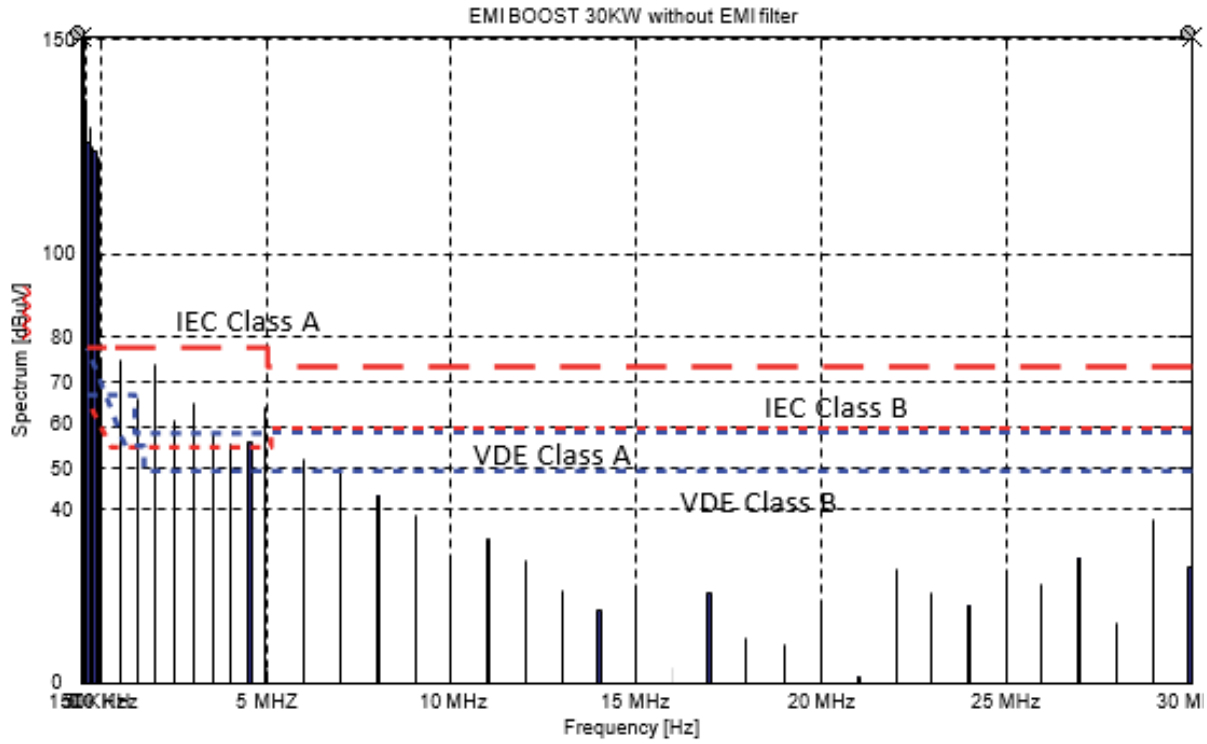

Figure 17: Results of the boost DC/DC converter EMI simulation

5.3 Interleaved 4-channel DC/DC converter

Figure 18 illustrates a simple four-level interleaved step-up converter, in which the inductances L1 through L4 are constructed by a distinct magnetic core. The gate signals to the power switching devices are phase-shifted using the formula T/N, where T is the switching period and N is the number of channels. One gate signal is phase-shifted after the other. Thus, with a ripple content of period T/N, every basic step-up converter level shares equitably in the current provided by the electric source (Destraz et al., 2006).

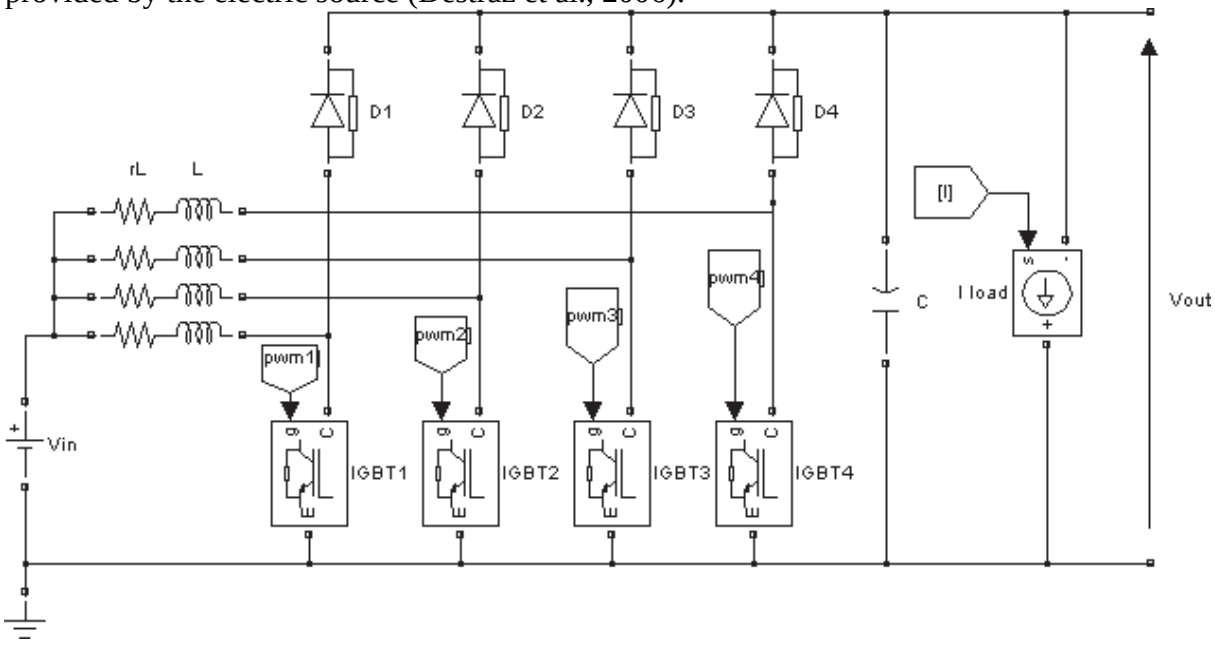

Figure 18: 4-channel step-up DC-DC converter that is interleaved

(a). The output voltage control loop is shown is Fig. 19.

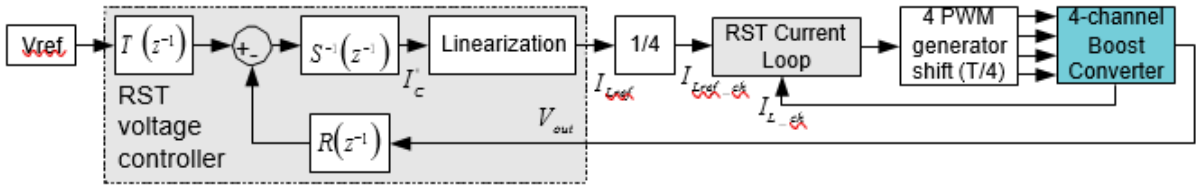

Figure 19: 4-channel voltage control loop for converter output

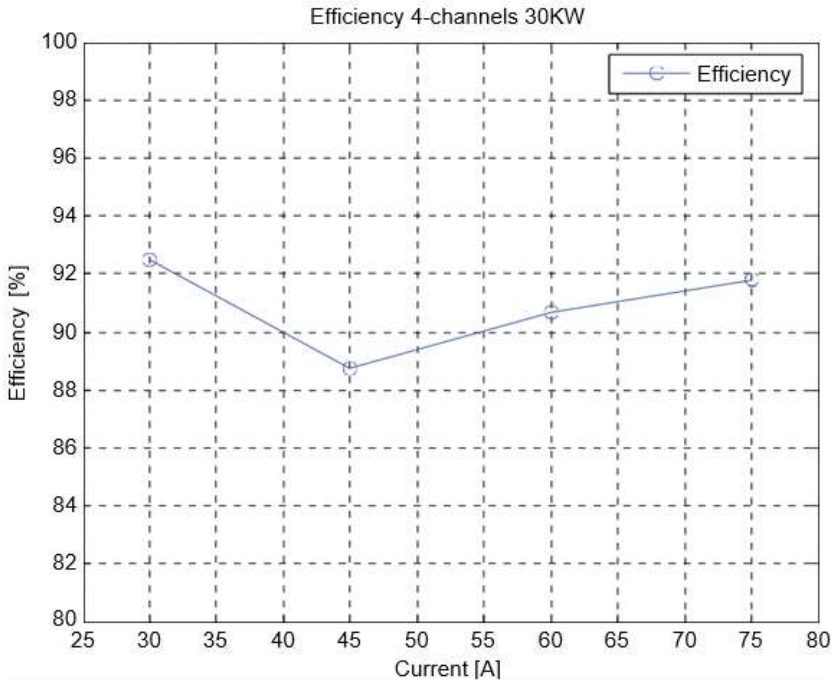

Figure 19: 4-channel converter performance in relation to current load

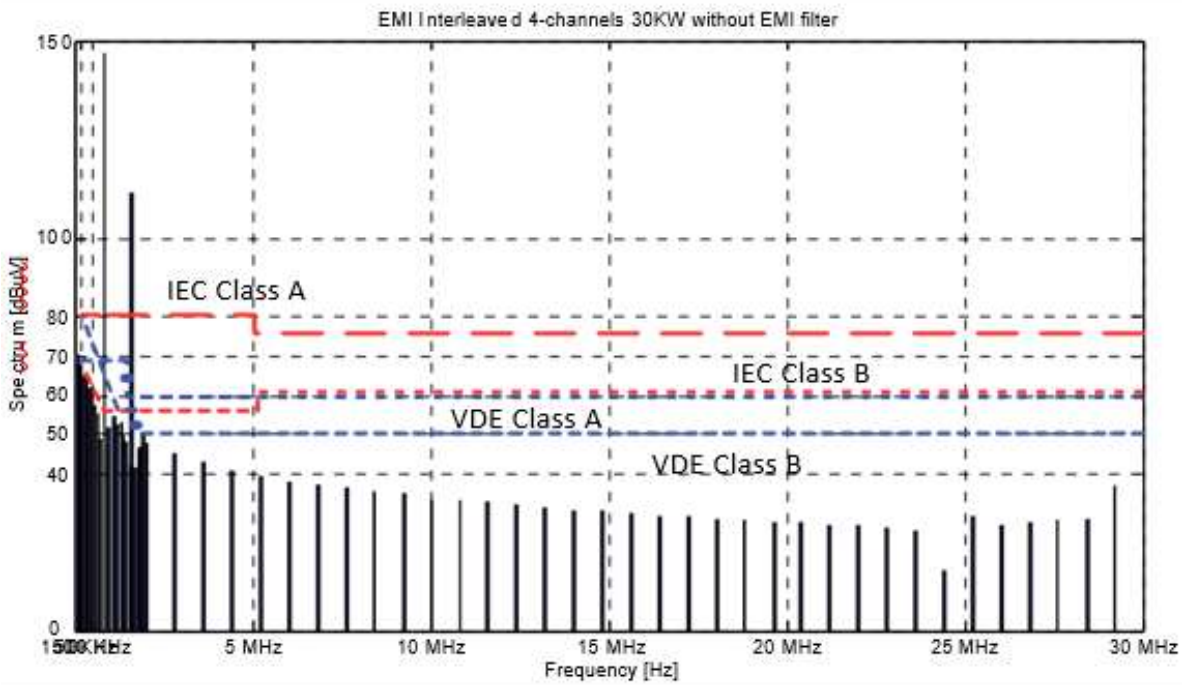

Figure 20: Results of an interleaved 4-channel DC/DC converter's EMI simulation

5.4 Full-bridge DC/DC converter

The structure of topology is seen in Figure 21. It is necessary to compute the transformer turns ratio n with respect to the minimal input voltage (Pepa, 2004).

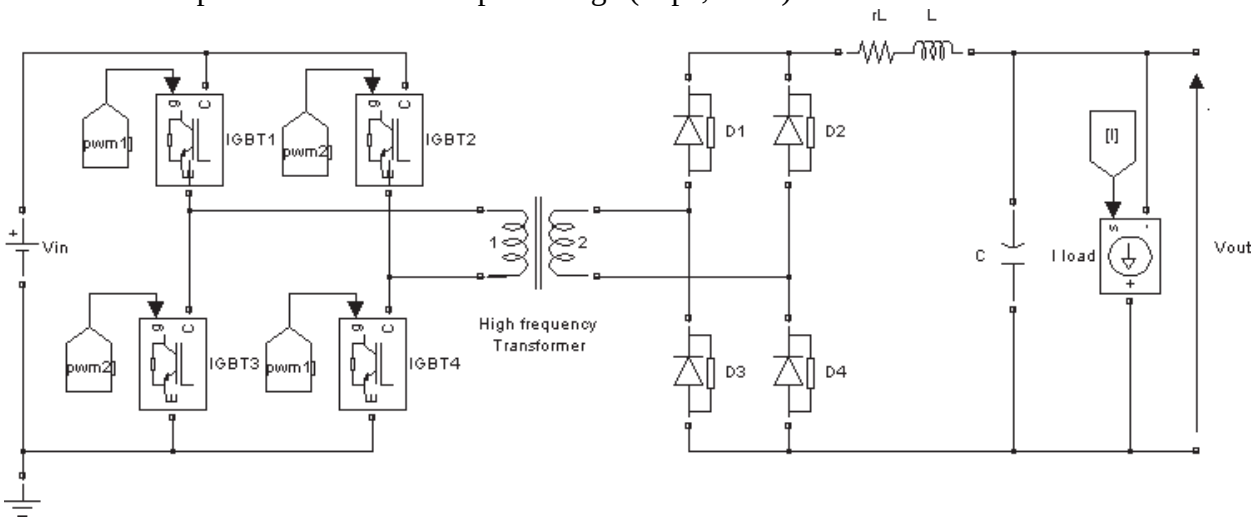

Figure 21: Step-up DC-DC converter with full bridge

(a). The inductor current loop is shown in Fig. 21.

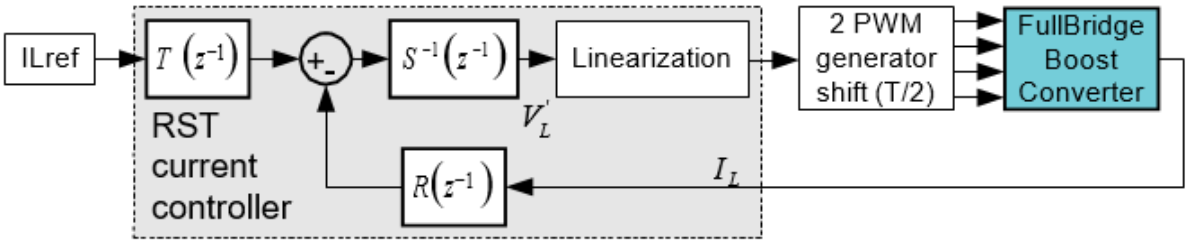

Figure 21: Current control loop for inductor in a full-bridge converter

(b). The output voltage control loop is shown in Fig. 22.

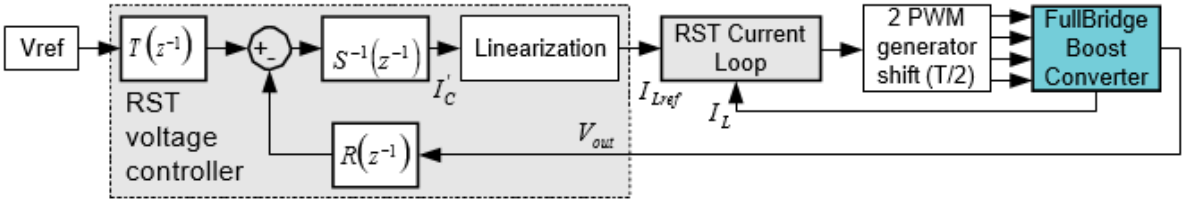

Figure 22: Voltage control loop for full-bridge converter output

Simulation results

The efficiency of the full-bridge dc/dc converter is around 91.5% at full load, as shown in Fig. 23. The efficiency of this converter can be increased via phase-shifted PWM control and zero voltage switching (ZVS).

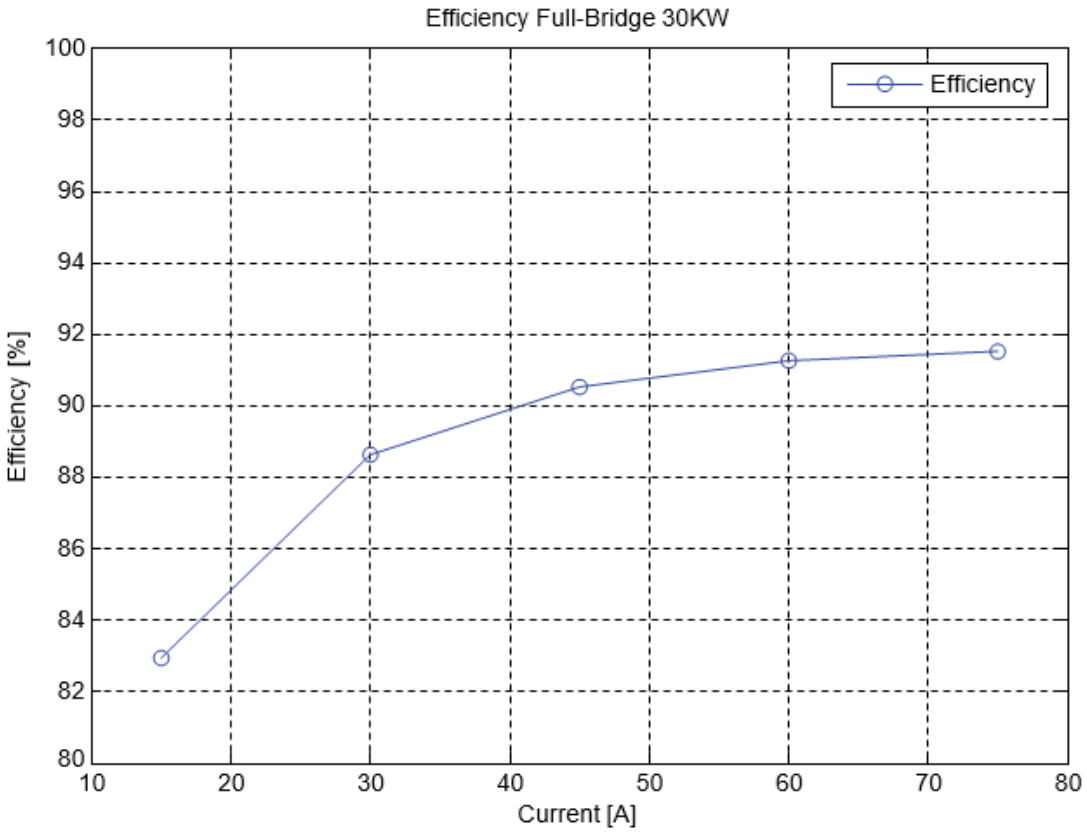

Figure 23: Efficiency of full-bridge converters in relation to current load

Fig. 24 displays the Full-Bridge converter's EMI spectrum. The level of conducted interference is prohibited by the limits. Therefore, suppression of the EMI filter is necessary to meet regulatory requirements.

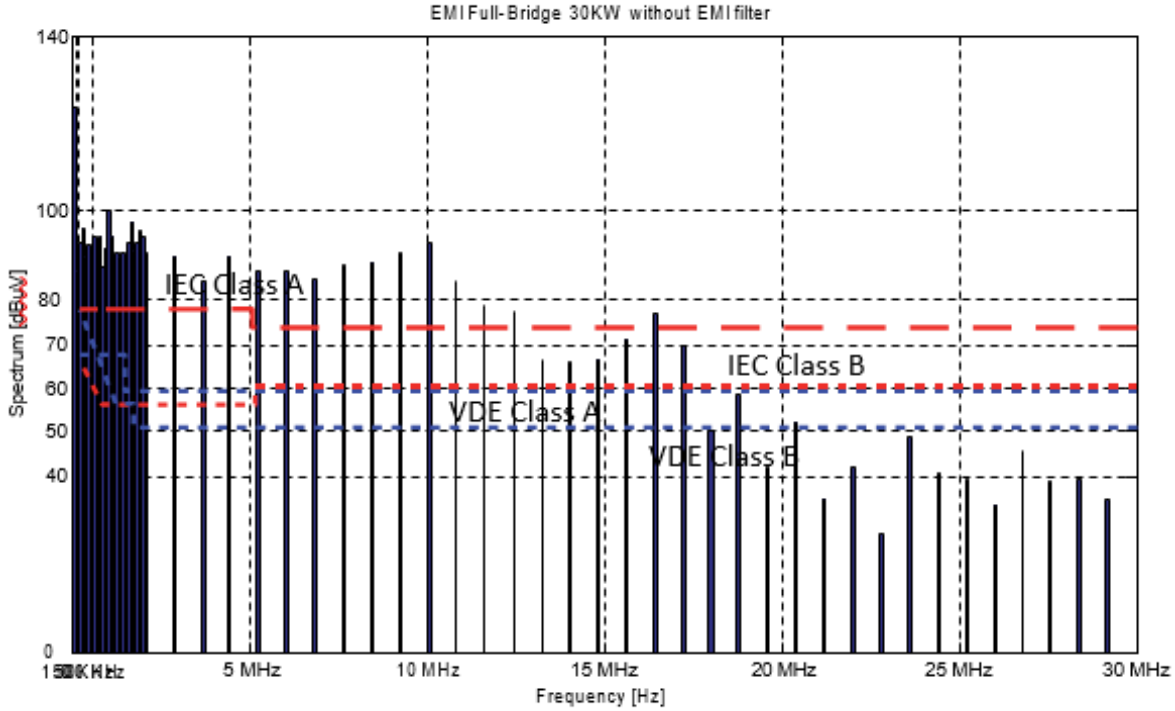

Figure 24: Results of the Full-Bridge DC/DC converter's EMI simulation

6. Interpreting & comparing results

Table 2 lists each converter's volume, weight, efficiency, and electromagnetic interference. The weight and volume of the inductor were estimated. Because of the output inductance, The full-bridge converter is clearly the largest in terms of weight and capacity. By increasing the converter's switching frequency, this inductance value can be decreased. It is evident that the Interleaving multi-channel architecture, with greater efficiency and reduced weight and volume, is the ideal choice for this application. The cooling system and the configuration of the components inside the converter enclosure are not taken into account during the weight and volume calculation procedure; only the IGBT, DIODE, Inductor, and Capacitor (the transformer for a complete bridge) are.

DC/DC converter	EMI	Volume(cm3)	Weight(g)	Efficiency at full load
Boost	-+	2167	6325	83%
Interleaved 4-channels	+	1380	3900	92%
Full-Bridge	--	3033	9268	91.5%

Fig. 25 Provides information on the variations in each converter's weight, volume, and efficiency.

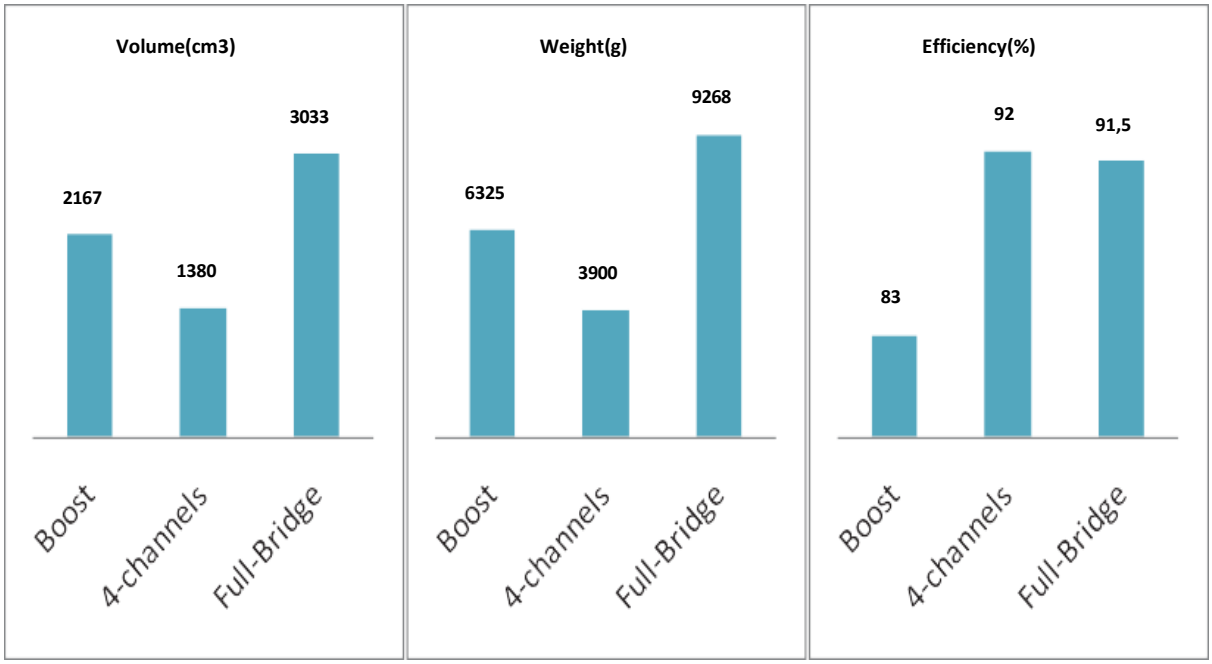

Figure 25: Efficiency as well as each converter's approximate weight and volume

7. Simulation

Throughout the design process, many simulations were conducted to verify design equations, ascertain ideal values of parameters not specified in the data-sheet, and obtain information from challenging expressions. The final simulated scheme that we employed is the one shown in Figure X. The previous simulation was tested on this schematic. The schematic operates the converter at three distinct input voltage levels (200V, 316V, and 400V) and 5 different load values i.e. (0%, 25%, 50%, 75%, and 100%). It should be mentioned that because to problems with simulation, the schematic fails to accurately represent the final design. The initial difference is that, due to simulation failures that sometimes caused the different protection circuits to be triggered in ways we do not anticipate occurring in real operation, Most of the non-critical set resistors and the OC were not utilized. The fact that a large number of the mosfets are not typical of the real mosfets we used is the second difference. This is because LTSpice models were not available for the majority of the mosfets that we used. The most noticeable of these is the primary mosfet, which incorporates an auxiliary boost converter. The switch timing resistors were not used as the timings would not be representative of the real system. Third, the addition of the input filter network would only lengthen the simulation duration because supply makes an excellent voltage source for simulations. Finally, the simulation does not contain the gate driver.

Through simulation, we were able to confirm the sustained effectiveness of the clamp and snubber network at 300 kHz, 500W. Furthermore, we found that a turns ratio of 4 and a primary inductance of 200 uH were the best configurations for the primary transformer. When this optimal location had been removed from, the clamp network ceased to operate at its best, increasing losses. Furthermore, we discovered that lowering the primary mosfet's current sense resistor significantly increased efficiency and enhanced performance at higher power. In the end, we were able to determine the average winding currents—a crucial piece of knowledge for calculating the winding losses of the transformer. The components of the optoisolator, sync transformer, and housekeeping supply were found to have no appreciable impact on performance. At its apex, our best simulation had an efficiency of 94.5%.

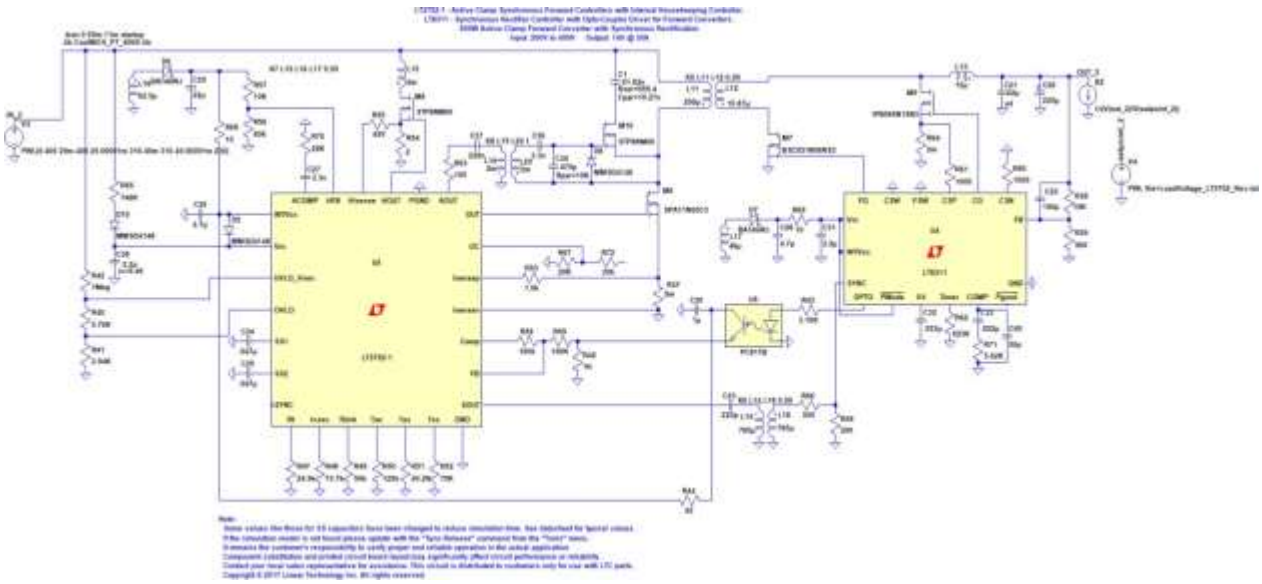

Figure 26: Final Simulation

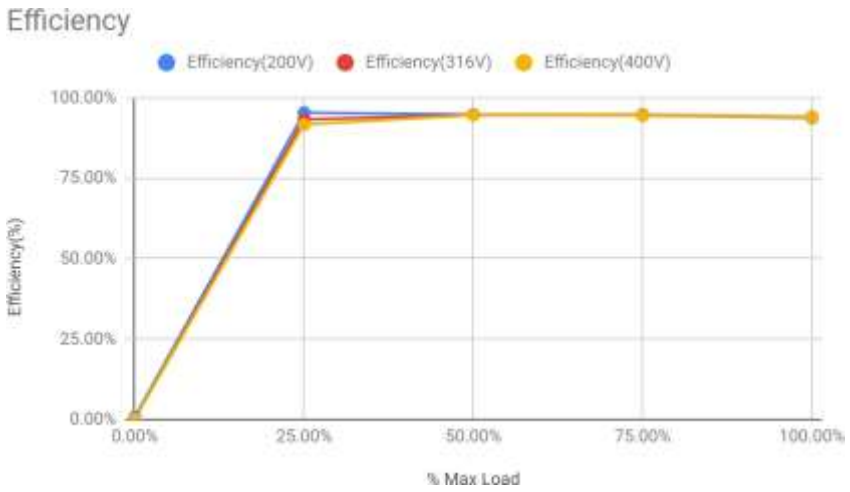

Figure 27: Efficiency Plot for Optimal Configuration

7.1 Transformer Design

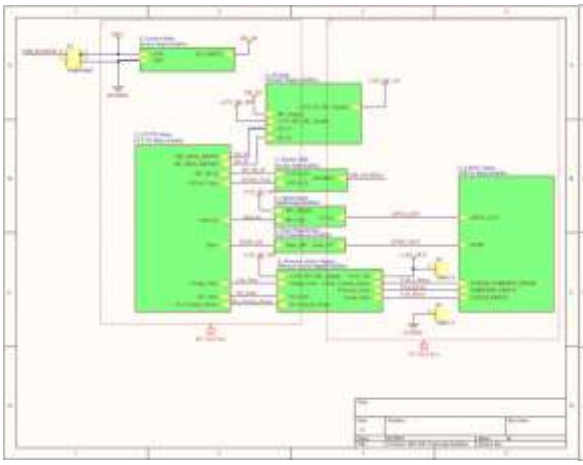

Figure 28: Schematic for DC-DC Top

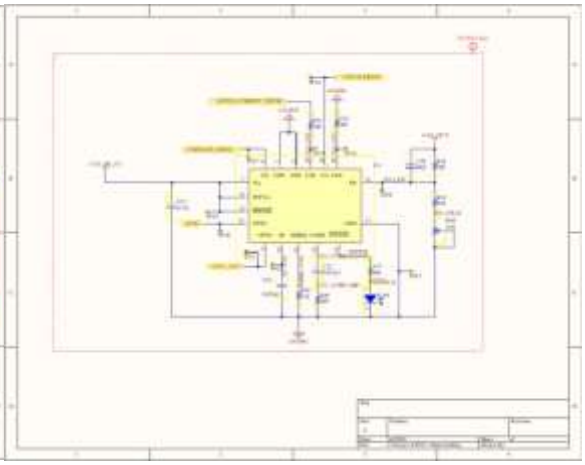

Figure 28: Schematic for LT8311

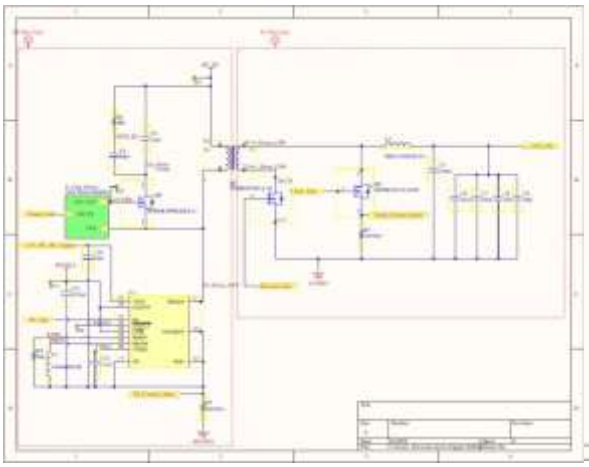

Figure 29: Schematic for Forward Active

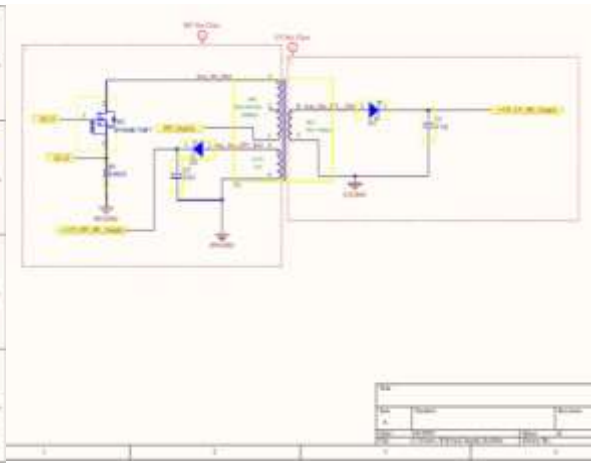

Figure 30: Schematic for Flyback

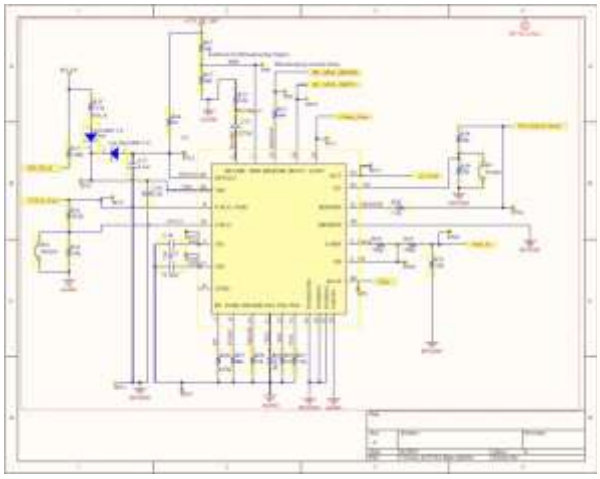

Figure 31: Schematic for LT3752-1

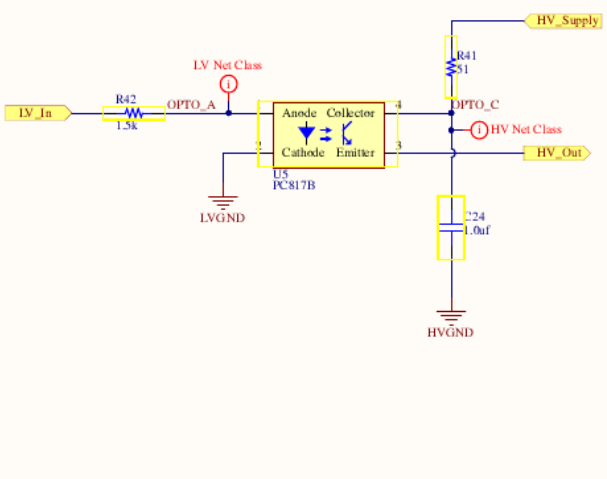

Figure 32: Schematic for OptoIsolator

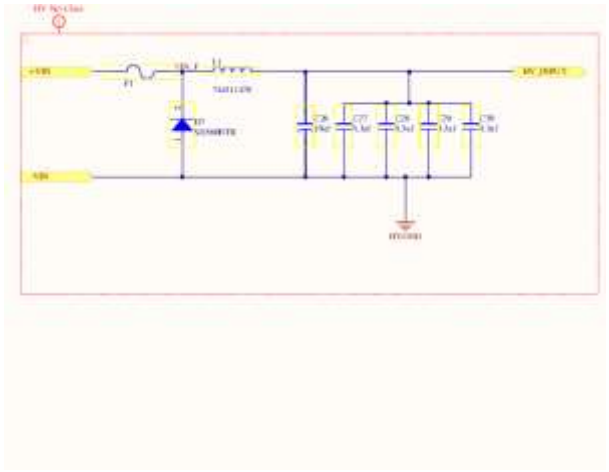

Figure 33: Schematic for Input Fusing and RVP

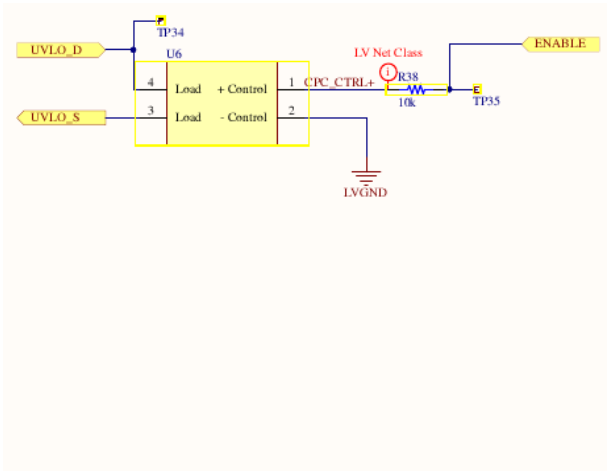

Figure 34: Schematic for DC-DC Disable

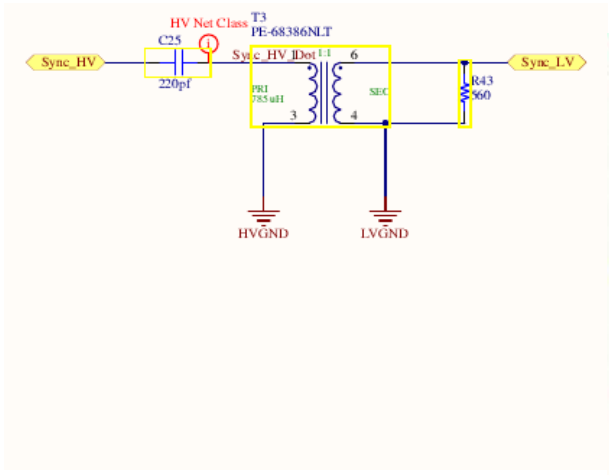

Figure 35: Schematic for Sync Transformer

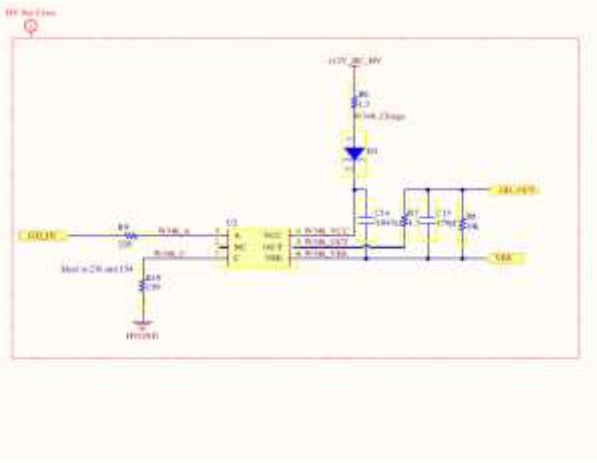

Figure 36: Schematic for Gate Driver

8. Hardware Test and Results

The main board and the transformer construction comprise the two distinct components of the DC-DC construction.

Furthermore, the inner layer will have a greater proximity effect resistance due to the gapping required to obtain the proper leakage inductance. Because the secondary winding suffers larger currents, it is therefore preferable to have it situated further from the core's center leg.

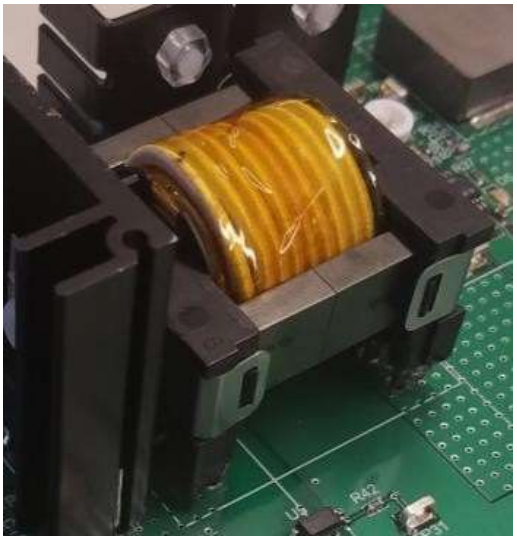

Figure 37: Final Constructed Transformer

We tested with two different transformer winding techniques, which we named low leakage and crossover. The low leakage winding method decreases the overall leakage inductance, but the crossover approach lowers the maximum voltage between neighboring windings. Since there are no discernible changes in Rac between the two ways, as Table 3 demonstrates, we have chosen to employ the crossover winding method to lower the danger of arcing in the transformer.

The projected values of the primary side inductance were nearly matched. With the chosen 0.2 mm gap, we were able to acquire our main side inductance of around 454uH, which is close to the projected 400uH. Since the datasheet lacked information on gaps formed by mixing disparate gaps, we examined every possible combination of gaps. We found that the primary side inductance that was closest to 200uH was generated with a 0.4mm overall gap. However, Rac measurements showed a considerable deviation from the computed results. The majority of Rac values were discovered to be more than 30 times higher than anticipated.

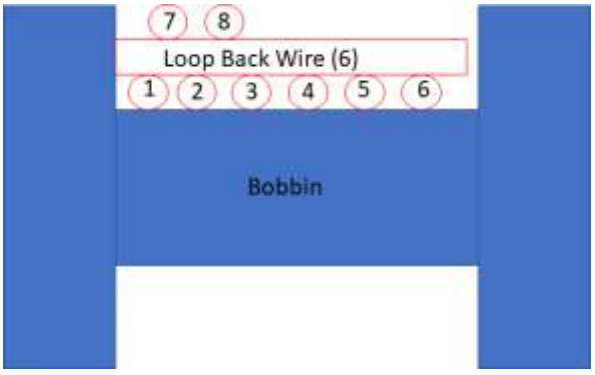

Figure 38: Low Leakage Winding Depiction

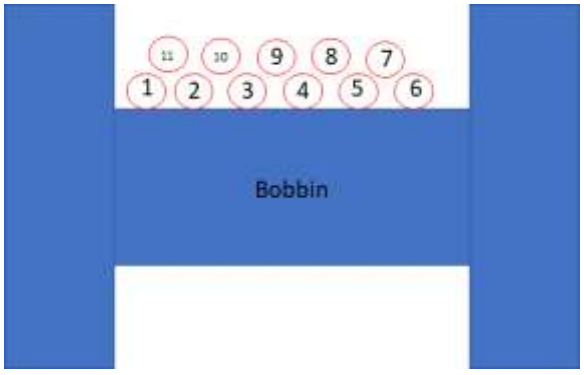

Figure 39: Crossover Winding Depiction

Table 3: Transformer Designing Test Data

Primary Winding Gap	L@300kHz (uH)	Rac@300kHz	Rdc (mOhm)	Winding
.4mm gap	268.8	2.2	Not Measured	Lleak attempt
.3mm gap	334	2.436	Not Measured	Lleak attempt
.2mm gap	454.6	3.097	Not Measured	Lleak attempt
.1mm gap	721	5.3	Not Measured	Lleak attempt
0 gap	2.5	123	Not Measured	Lleak attempt
.4mm gap	269	2.53	50.93	Crossover
.3mm gap	336.3	2.77	50.93	Crossover
.2mm gap	454.2	3.6	50.93	Crossover
.1mm gap	709	6.8	50.93	Crossover
0 gap	2.49	124.4	50.93	Crossover
Secondary Winding				
.4mm gap	21.09	0.3439	4.065	
Calc'd N1/N2	3.571394703			

The primary board of the DC to DC converter is designed using Altium Designer; Figures 40, 41, and 42 display the board layout and design. The VIN and GND of each integrated circuit were in close contact to decoupling capacitors. On the LT37352-1, the resistors TAO, TAS, TOS, TBLNK, IVSEC, and RT were positioned in close proximity to each pin. LT3752-1 Pin 18 was grounded by means of a single, closed-off AGND aircraft. Using Kelvin connections, the ISENSEP and ISENSEN pins of the LT3752-1 were linked to the main current sense resistor. In addition, the ground connection of the housekeeping supply's current sensing resistor was near pin 38, PGND. In order to get the MOSFETs closer to the LT3752-1, The gate driver minimized the length of the HOUT, AOUT, SOUT, and OUT traces. To lower current path resistance, high current traces have been broadened and coupled via vias on several levels. In order to comply with to Formula SAE regulations, Additionally, the PCB's low and high voltage components were spaced apart by at least 4 mm.

The board was intended for a four-layer, one-ounce PCB. Bay Area Circuits etched the PCBs after the layout was complete. In order to reduce manufacturing time, homemade stencils were

constructed to solder the board. Two thicknesses of Kapton tape adhered to opposite sides of a sheet of paper served as the basis for the stencil. The Altium board layout's paste layer was then used to cut the Kapton-paper composite with a laser cutter, creating a temporary stencil. Using a toaster oven and a microscope, After the solder paste had been deposited, all non-through-hole components were positioned on the top layer. The bottom layer and remaining through-hole components were soldered by hand. The heat sinks of the through-hole MOSFETs were fastened to the device with plastic fasteners and nuts with thermal pads for insulation.

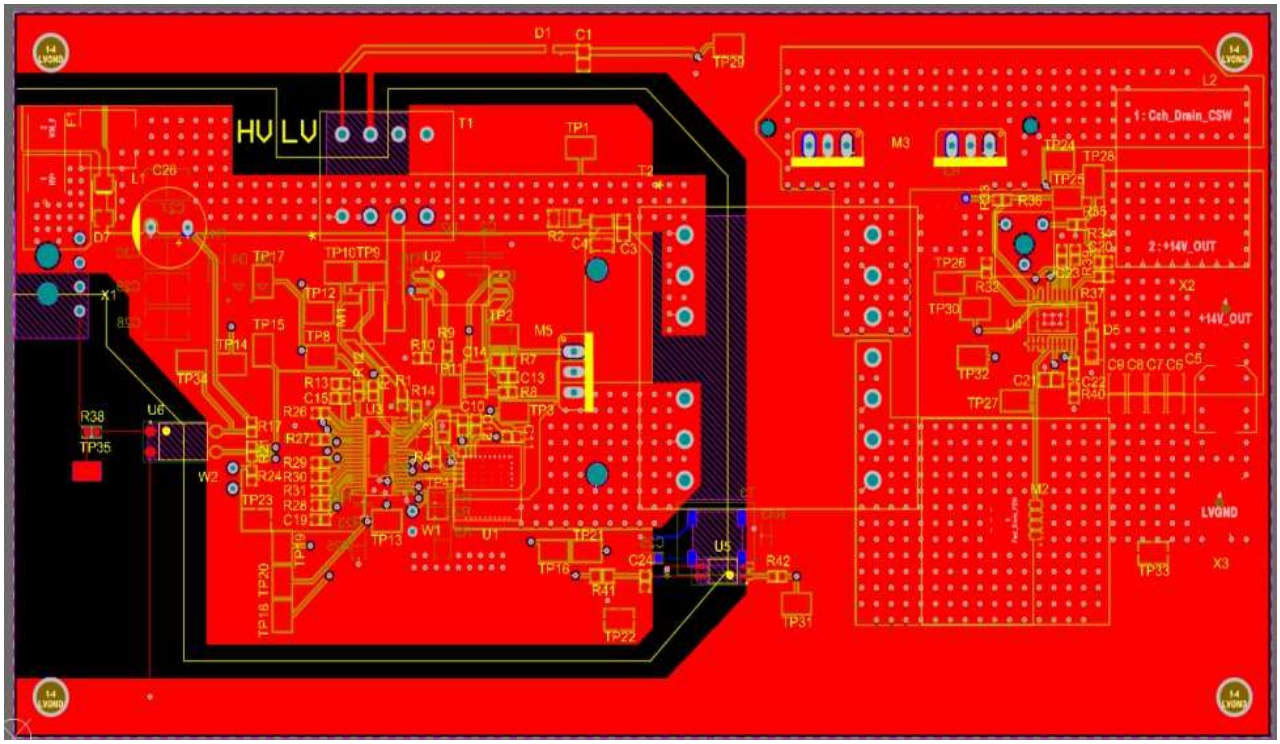

Figure 40: DC-DC Main Board Layout

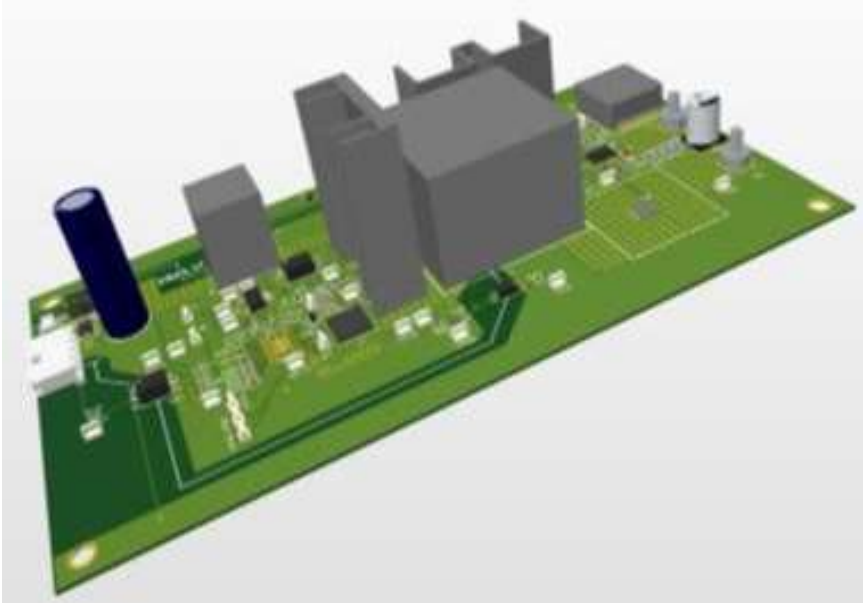

Figure 41: DC-DC 3D Render

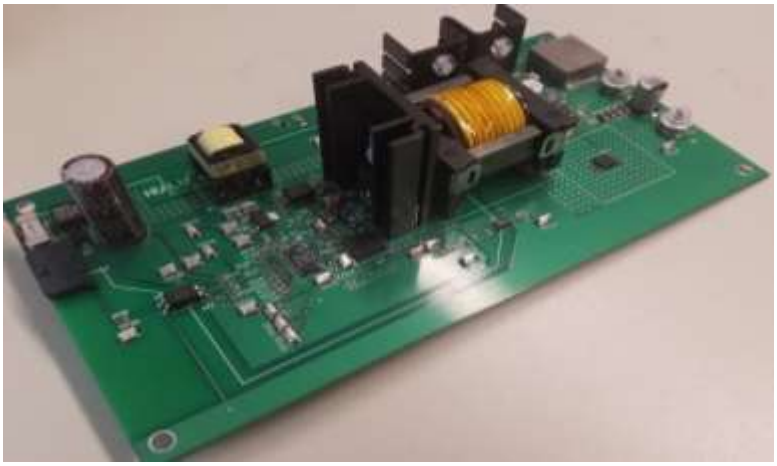

Figure 42: DC-DC Final Construct Board

Several oscilloscopes and differential probes were used to measure and characterize the converter in order to sufficiently monitor all crucial signals and rails. The basis of the test setup was the monitoring of the input and output voltage and current. The final test setup, as seen in Figures, employed two parallel 600V, 1.5A power supplies to source the converter. The HV current line, which also went via an ammeter, ended at the DC-DC converter. Following the installation of the input fuse, the input voltage of the DC-DC converter was also checked using a multimeter to see if it had exceeded its overcurrent limit. An extra multimeter was utilized to measure the output voltage and an electronic load from BK Precision was used to evaluate the output current after the converter was loaded.

We were unable to precisely describe the DC-DC converter's operation because of several failures. As at the time of writing, the DC-DC converter was experiencing excessive ringing, which ultimately caused the converter to fail.

Table 4: Efficiency Test Result

Input Voltage	Load	Efficiency	Output Voltage
200V	0%	N/A	9V
200V	25%	93%	7V

9. Conclusion

This project describes the design and construction of the HV (High Voltage) to LV (Low Voltage) DC-DC converter for the Formula SAE Student Design Competition (FSAE) electric motor cars. The finished DC-DC converter successfully demonstrated a high frequency power transformer design, providing additional helpful framework to speed up the development of further DC-DC projects. A few issues surfaced during the testing of the converter, including exceeding load requirements due to excessive ringing on the main and secondary sides, which finally led to the power MOSFETs breaking at low loads. Other lessons learned from this project include the information needed to choose a heatsink appropriately and balance switching and conduction losses to maximize efficiency. Finally, we have created a measuring system to make it easier to synchronize several oscilloscopes for differential probe measurements.

Three different DC-DC converter topologies are shown in this paper: full-bridge step-up DC/DC converter, interleaved step-up DC/DC converter, and boost DC/DC converter. Basic interleaving technology forms the backbone of the second construction, whereas a simple, single step-up converter is considered in the first. Even though it is simple, this structure reduces weight and volume while improving the quality of the step-up converter used for obtaining electricity from the fuel cell. It does, however, have limitations when high voltage step-up is needed. The third topology is the full-bridge converter, which enables high voltage step-up by use of a high frequency transformer. There are simulations conducted on three 30 KW converters. The simulations contain real components (IGBT and Diode); the weight and volume of each converter were calculated using datasheets. Every converter's efficiency was determined under the worst-case scenario, which involves the greatest losses in the power switches. Interleaved 4-channel DC/DC converters are the optimum option for this application, according to simulation results. It is more efficient, requires less volume and weight, and has less electromagnetic interference (EMI).

The frequency of the ringing decreased when the output inductor value was increased, suggesting that a larger output inductance might also be beneficial. According to the Demo Board results, the voltage at the top leg of the transformer computed the upper half of a sine wave with audible ringing. This shows that two resonances are superimposed: one at a higher frequency and the other at a lower frequency. The higher frequency resonance is associated with switching or leaking inductance, while the lower frequency resonance is related to the resonance between the output capacitance and output inductor.

Ongoing testing & validation of the transformer is required as an additional enhancement. Without the required testing facilities, we were unable to assess our transformer's capability for power handling, load control, and leakage inductance. Transformer characterization is important because high secondary side leakage inductance might limit the ringing to the secondary side. A fixed time active clamp forward converter or an H-bridge might make it simpler to determine what's causing the ringing.

Water cooling could be added to further minimize size by reducing the amount of cooling effort needed. Because switching energy would drop as a result, designers will be able to use smaller switching integrated circuits, which should increase efficiency. Additionally, this would reduce the overall mass needed for heatsinks.

A complete microcontroller system addition is another possible enhancement. This would greatly increase the design's flexibility and the quantity of telemetry that could be returned. It was difficult to transfer the voltage and current sensor data from this project to an external processor. In addition, the output voltage was limited to manual adjustment. A microcontroller system could be used for both of these tasks.

Developing one's skills in power electronics, automated testing, environmental-rated components, magnetic design, isolated power supply design, and thermal dissipation in electronics will be necessary for this project.

10. References

[1] L. McDonald, CleanTechnica, January 13, 2019, "US EV Sales Surpass 2% In 2018 — 9 EV Sales Charts." [Online]. The following link is available: https://cleantechnica.com/2019/01/12/us-ev-sales-surpass- 2-for-2018-8-more-sales-charts/.

[2] "EV-1 White Paper," September 11, 2002. [Online]. Available at http://www.cleanup-gm.com/ev1.html and https://web.archive.org/web/20090726034344.

[3] "Tesla's Model 3." [Online]. https://www.tesla.com/model3 is accessible.

[4] N. Sridhar, "Using High-Voltage Solutions to Drive the Future of HEV/EV." [Online]. http://www.ti.com/lit/wp/slyy052b/slyy052b.pdf is accessible.

[5] "Hybrid Electric Vehicle and EV: DC-DC converter," 2013.

[6] "Internal Housekeeping Controller with Active Clamp Synchronous Forward Controllers, LT3752/LT3752-1." [Online]. [https://www.analog.com/media/en/technical-documentation/data-sheets/3752fb.pdf] is the link that is available.

[7] "LT8311 Opto-Coupler Driver for Forward Converters and Synchronous Rectifier Controller." [Online]. https://www.analog.com/media/en/technical-documentation/data-sheets/8311f.pdf is the link that can be accessed.

[8] "MANUAL DC1929A LT3752-1/LT8311 200W Active Clamp Forward Converter with 150V to 400V Input Voltage Demo." [Online]. https://www.analog.com/media/en/dsp-documentation/evaluation-kit-manuals/dc1929afa.pdf is the link that can be accessed.

[9] "Integrated GaN power stage with overcurrent protection, LMG341xR050, 600-V, 50-mΩ." [Online]. https://www.ti.com/lit/ds/symlink/lmg3410r050.pdf is accessible.

[10] "LT3752 LT3752-1 Product Details and Datasheet | Analog Devices." [Online]. https://www.analog.com/en/products/lt3752.html#product-tools is the URL that is accessible.

[11] "Design of Power Transformers." https://www.ti.com/lit/ml/slup126/slup126.pdf is the URL that can be accessed online.

[12] "FSAE Regulations." [Online]. The website https://www.fsaeonline.com/page.aspx?pageid=e179e647-cb8c-4ab0-860c-ec69aae080a3 is accessible.

➢ Modelling Pics of DC-DC Converter for Electric Vehicle by Using Matlab

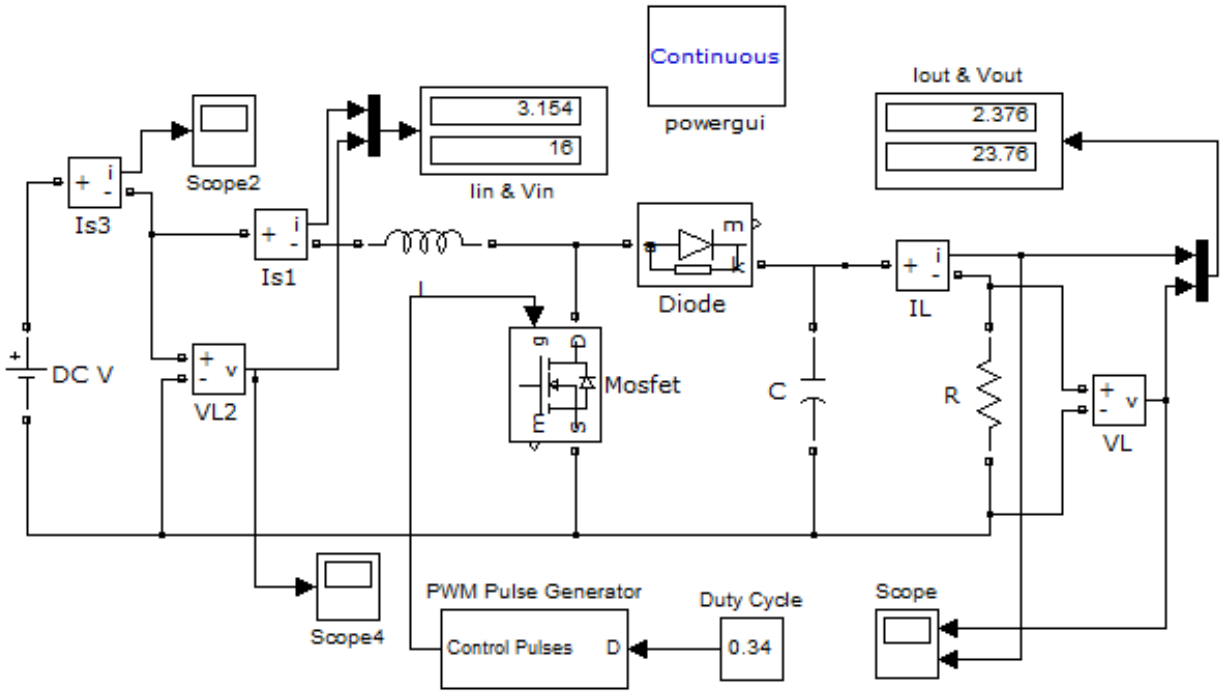

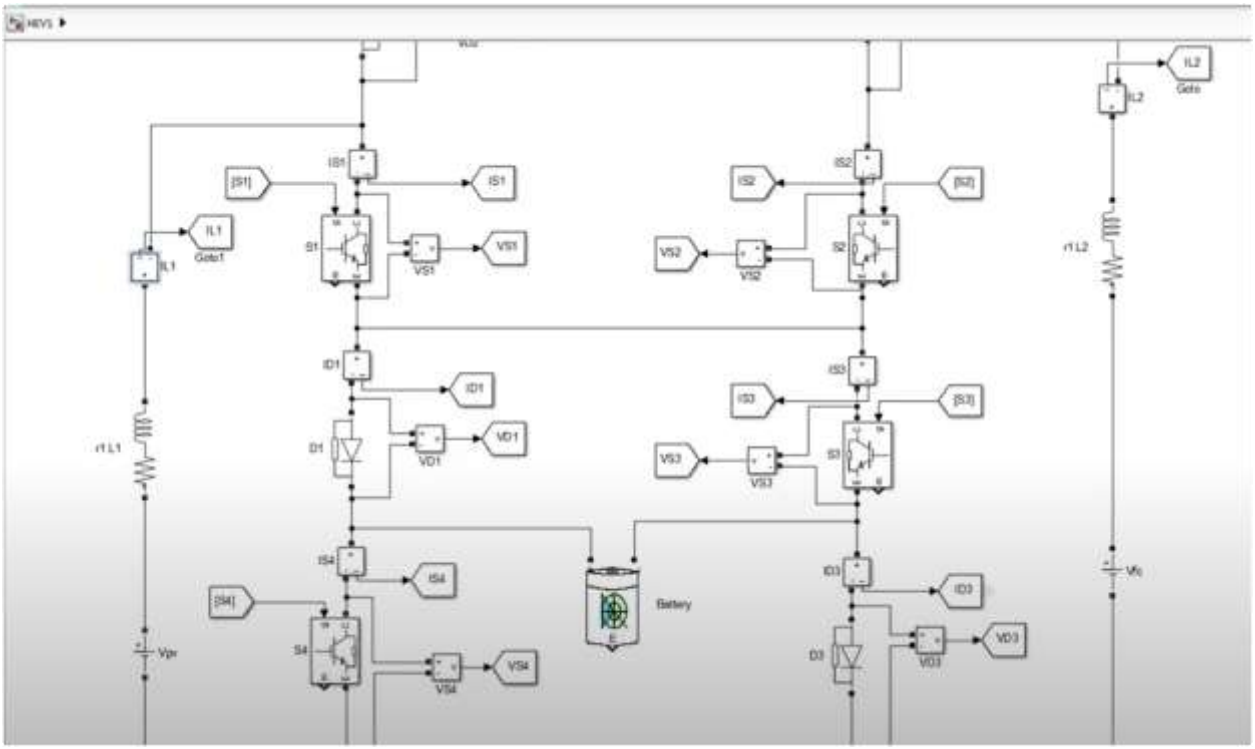

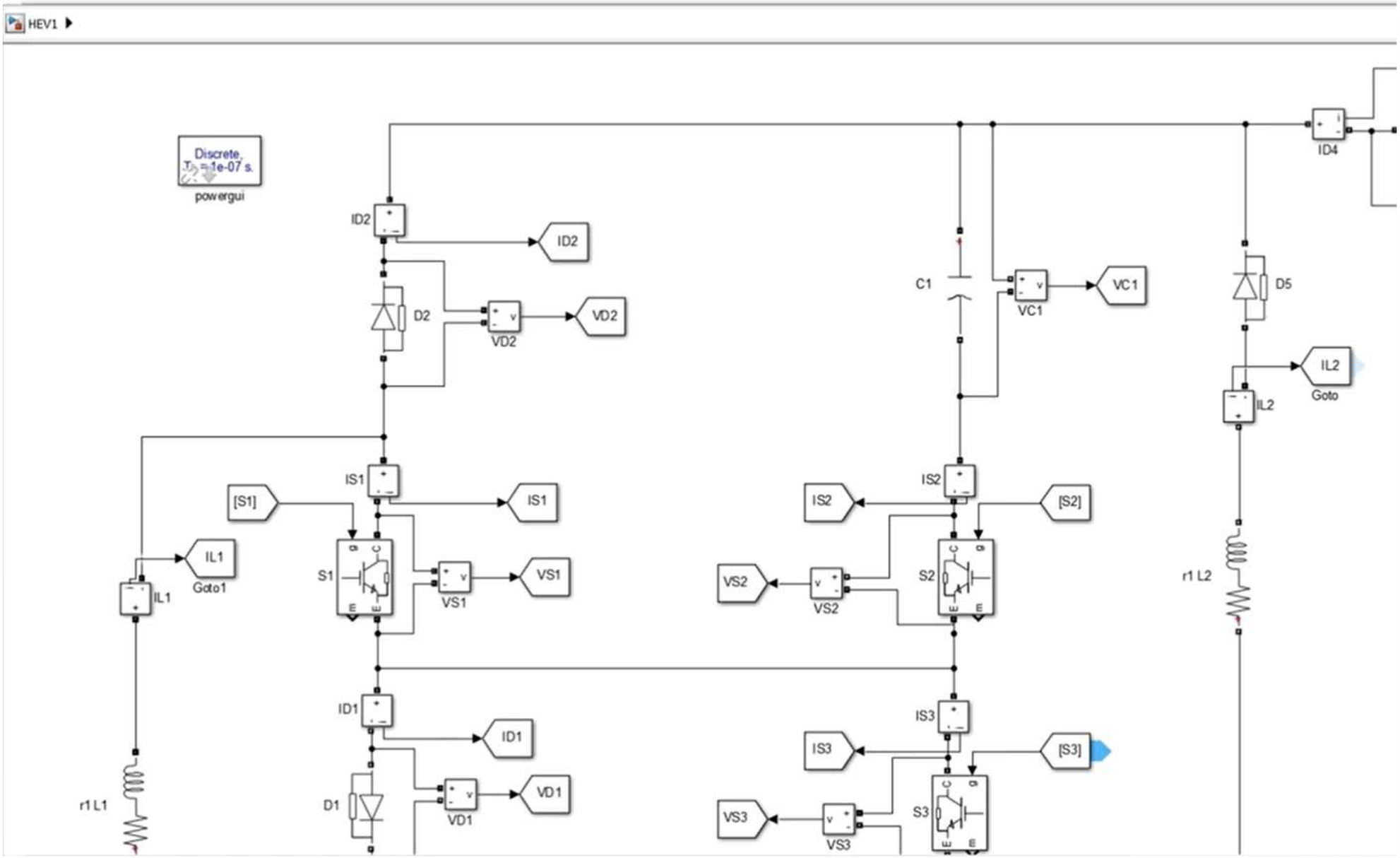
HEV1
Discrete,
Ts = 1e-07 s.
powergui
ID2
ID2
D2
VD2
VD2
C1
VC1
VC1
ID4
D5
IL2
Goto
IL2
r1 L2
IS1
[S1]
IS1
IL1
Goto1
IL1
S1
VS1
VS1
IS2
IS2
[S2]
VS2
VS2
S2
ID1
ID1
D1
VD1
VD1
IS3
IS3
[S3]
VS3
VS3
S3
r1 L1

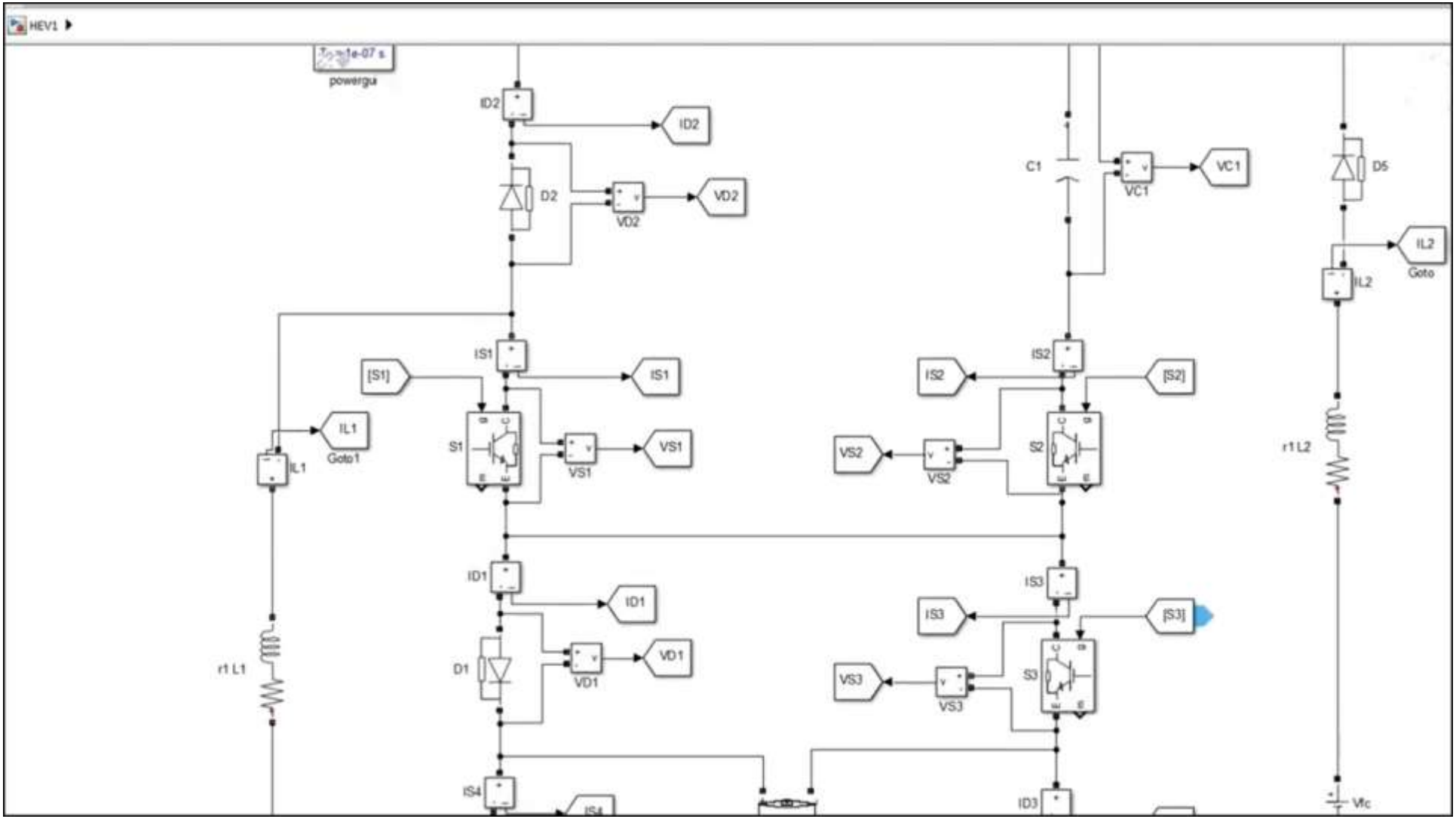
HEV1
powergui
ID2
D2
VD2
C1
VC1
D5
IL2
Goto
IS1
[S1]
S1
VS1
IL1
Goto1
IS2
[S2]
S2
VS2
r1 L1
r1 L2
ID1
D1
VD1
IS3
[S3]
S3
VS3
IS4
ID3
Vfc

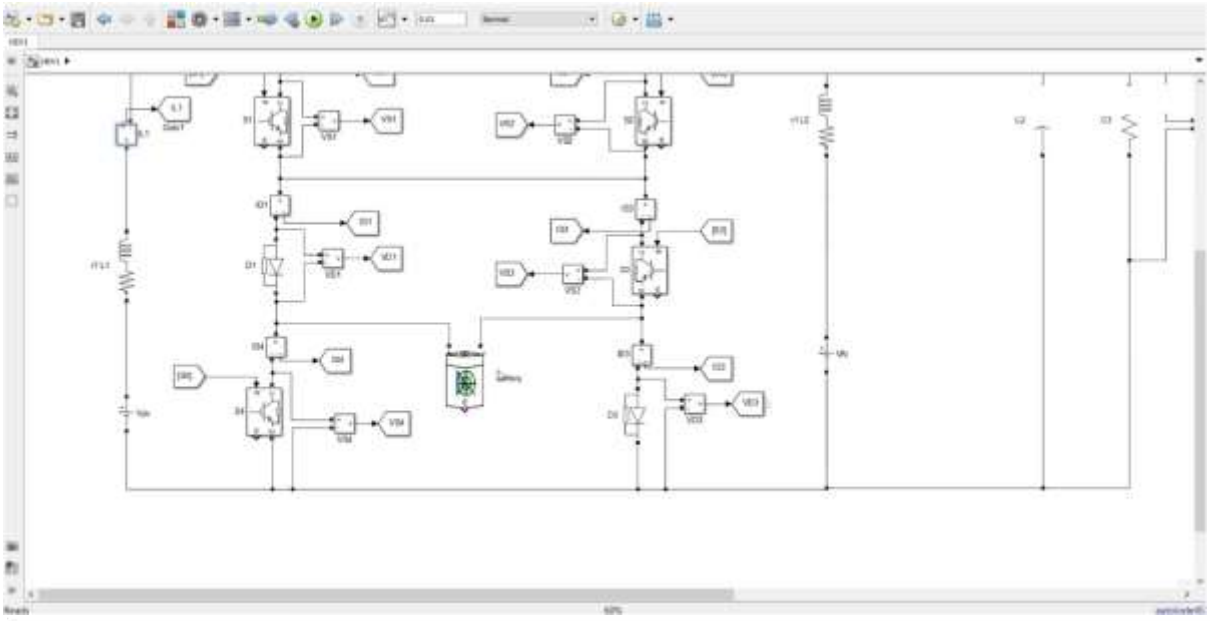

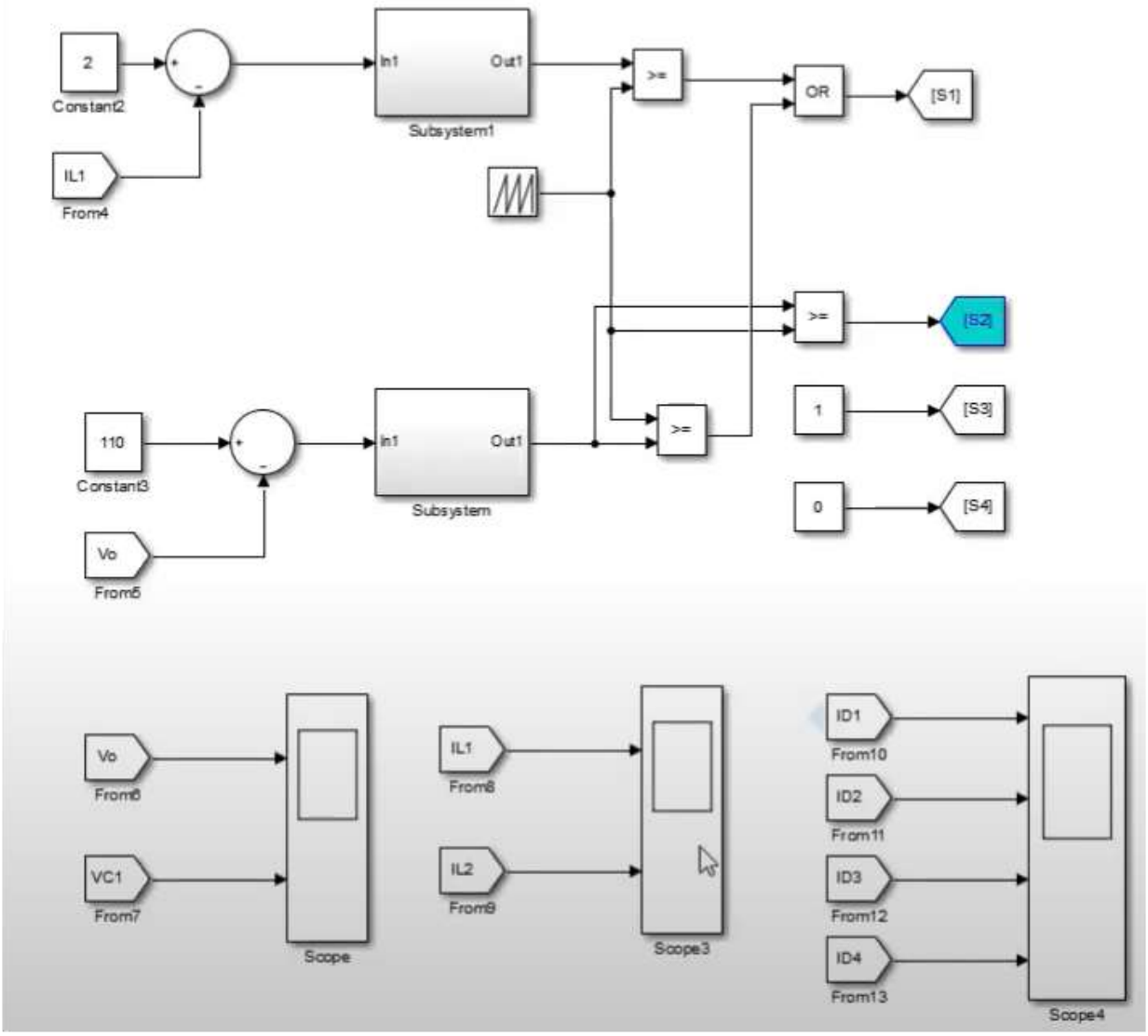
2
Constant2
IL1
From4
In1
Out1
Subsystem1
>=
OR
[S1]
>=
[S2]
1
[S3]
0
[S4]
110
Constant3
Vo
From5
In1
Out1
Subsystem
>=
Vo
From6
VC1
From7
Scope
IL1
From8
IL2
From9
Scope3
ID1
From10
ID2
From11
ID3
From12
ID4
From13
Scope4